NONDESTRUCTIVE STRESS MEASUREMENT OF CARBON STEELS UTILIZING MAGNETO-STRICTION(Dissertation_全文)

AUTHOR(S):

Utsunomiya, Tomoaki

NONDESTRUCTIVE STRESS MEASUREMENT OF CARBON STEELS UTILIZING MAGNETOSTRICTION

BY
TOMOAKI UTSUNOMIYA

DEPARTMENT OF ARCHITECTURAL ENGINEERING
KYOTO UNIVERSITY
KYOTO, JAPAN
JUNE 1990

NONDESTRUCTIVE STRESS MEASUREMENT OF CARBON STEELS UTILIZING MAGNETOSTRICTION

A THESIS SUBMITTED TO
THE FACULTY OF ENGINEERING
IN CANDIDACY FOR THE DEGREE OF
DOCTOR OF ENGINEERING

BY
TOMOAKI UTSUNOMIYA

DEPARTMENT OF ARCHITECTURAL ENGINEERING
KYOTO UNIVERSITY
KYOTO, JAPAN
JUNE 1990

ACKNOWLEDGMENTS

The author sincerely acknowledges his indebtedness to Dr. Kiyoshi Kaneta, Professor of Kyoto University, for his continuous guidance and encouragement throughout this study. A grateful acknowledgment is made to Dr. Hidekazu Nishizawa, Research Assistant of Kyoto University, for his kind introduction to this research field and his invariable encouragement. The valuable suggestions of Dr. Isao Kohzu, Assistant Professor of Kyoto University, and Mr. Keiichiro Suita, Research Assistant of Kyoto University, are likewise highly appreciated.

The author is thankful to Mr. Hideo Sawamura and Mr. Tunekiyo Fuse, Technical Officials of Kyoto University, for their assistance in carrying out the experiments. The implementation of the the experiments had been possible through the help of Mr. Hideaki Kondo, Research Engineer of Nikkosi Co., Ltd., and Mr. Tomohiro Ozawa, former graduate student of Kyoto University. Acknowledgment also goes to Mr. Hiromasa Takeno, Research Assistant of Kobe University, and Mrs. Cynthia L. Muncada, graduate student of Kyoto University, for their kind suggestions in writing the manuscript.

Part of this research has been carried out under the award from the Japan Society for the Promotion of Science (JSPS).

TABLE OF CONTENTS

CHAPTER I

GENERAL INTRODUCTION

Steel structures such as bridges, buildings, towers, pressure vessels, etc. have been designed and constructed on the basis of stress analyses utilizing simplified models. Unfortunately, the actual state of structures is rather complicated; there is usually a discrepancy between the analyzed stresses and the actual stresses. For example, residual stresses often exist in the materials even when the applied load is zero, or the assumed loading conditions may differ from the actual loading conditions because of their complications. In some cases, the collapse of the structures arise from the incompatibility between the analyzed stresses and the actual ones. If we can precisely measure the actual stresses, such collapse will be predicted and prevented.

For some structures where stresses are applied repeatedly, fatigue fractures can occur at stress levels well below the tensile strength. Fatigue fractures are known to be affected by residual stresses, i.e., compressive residual stresses lengthen the fatigue life and tensile residual stresses shorten it. It is therefore important to estimate residual stresses in order to predict the fatigue life. For these reasons, the

development of techniques for precisely measuring stresses has been desired in the fields of structural engineering.

A lot of techniques for experimental stress analysis have already been developed. There are methods of photoelasticity, moire methods, brittle coating techniques, X-ray techniques, acoustic techniques, and electrical techniques such as strain gauges, etc. With regard to service structures, the present nondestructive techniques such as X-ray diffraction, acoustic, and magnetic techniques are used for measuring stress.

X-ray diffraction techniques have been the most well-established of the three methods [1]; however, their application to service structures is limited because these techniques require special technical skill [2]. It can only measure stresses in the surface layer of the order of 0.01 mm. Since the main concerns in the fields of structural engineering are the subsurface stresses distributed through the cross-section, the difference in the surveyed depth is thus one of the reasons why the X-ray diffraction techniques have seldom been used.

Acoustic techniques are based on acoustoelasticity, a phenomenon wherein ultrasonic elastic waves transmitted through a material are affected by stresses [3]. The difference of principal stresses can be measured by using the birefringent effect which is similar to photoelasticity. Unfortunately, because the stress-induced birefringent effect is very small (the relative change is on the order of 10^{-2} GPa^{-1}), other factors such as temperature, microinhomogeneity, texture, and weak anisotropy of a material cannot be neglected and the

measured stresses often indicate considerable errors. In fact, it has been shown that the residual stresses in a wide-flanged rolled beam measured by using this technique indicated considerable errors caused by the texture anisotropy [4]. It seemed difficult to reduce such errors within the acceptable limits.

Magnetic techniques are based on the magnetostriction effect, which is a phenomenon of elastic deformation of certain ferromagnetic materials, e.g., nickel and steel, with the application of magnetic fields. The inverse magnetostrictive effect, i.e., change of magnetization under applied stress, is often applied for a nondestructive stress measurement. Its application is, of course, limited to the measurement of ferromagnetic materials. However, its application to a stress measurement of steel has the following advantages:

(1) Subsurface stresses can be measured nondestructively.

(2) Variation of magnetization due to stresses is large (the relative change is on the order of 1 GPa^{-1}).

(3) Anisotropy of material is negligible for hot-rolled steel.

(4) The apparatus can be portable and the measuring speed is excellent.

Studies for measuring stresses in steel on the basis of magnetostriction have been performed by several authors and these will be reviewed. Azumi and Iwayanagi [5] and Osaki [6] developed a method for measuring tension in steel chords for prestressed concrete. They used a bridge circuit with two

magnetic probes: one is for measurement and the other for compensation. The advantages of this method are its easy handling, speedy measurement, and high accuracy. However, the output of the apparatus changes nonlinearly with tension, such that calibration tests are required for each measuring condition. This has therefore become less popularly used compared to the strain gauges currently used for this purpose.

The above mentioned method was extended to the case of measuring stresses in steel plates in order to estimate the dead load applied to steel structures [7]. The study included the influence of chemical compositions of specimens on the stress sensitivity. The results showed that the stress sensitivity considerably decreased with an increase of the carbon content.

Yoshinaga [8] reported a systematic study about the same method as [7]. He examined the factors affecting the magnetic output, the relationship between the magnetic output and uniaxial stresses of both tension and compression, and the relationship between the magnetic output and biaxial stresses. The results of the biaxial test showed that the principal direction and the difference of principal stresses could be measured by this method. The difference of principal stresses were separated into the principal stresses themselves by using the shear difference method, which is often used in the photoelastic stress analysis. Using this method, he measured the distribution of residual stresses around welds in steel plates.

There are some types of probe methods utilizing magnetostriction similar to the methods mentioned above. Abuku

[9] presented a magnetic probe which did not require compensating probes. He also examined the effect of plastic deformation to the magnetic output. Langman [10-13] reported independently the probe method based on the rotation of magnetic fields induced by stresses. Methods using magnetic probes have been remarkably improved and suited for engineering applications [14-19].

All of these probe methods are based on the change of magnetization in low magnetic fields. In this paper, low magnetic fields mean the fields where the change of magnetization is caused mainly by the displacement of domain walls (< 1 kA/m for iron), and high magnetic fields mean the fields where it is caused mainly by the rotation of magnetization vectors ($>$ 1 kA/m for iron). Because the theoretical treatment of the displacement of domain walls is complicated, it is difficult to predict the variation of magnetization caused by stresses in low fields. Some theories have already been proposed [20-24], but the quantitative agreement with the experimental results was not favorable.

In the methods utilizing magnetostriction in low fields, carbon content, plastic deformation, or heat treatment of materials exert influence on the outputs; these effects are undesirable when the methods are used for measuring stresses. The methods can measure only the difference of principal stresses in a biaxial stress state. The shear difference method is required to separate into the principal stresses themselves from those differences. However, it is applicable to only a few cases because of the integration error and/or nonexistence

of stress-free points near the measuring points.

The methods utilizing magnetostriction in high magnetic fields have also been studied. Iwayanagi and Abuku [25] indicated that in high fields the influence of carbon content on the stress sensitivity was considerably less than that in low fields. In another study, they also indicated that in high fields the influence of plastic deformation on the measurement of stresses was quite small [26]. The method in high fields was elaborated by Abuku and Cullity [27] and Iwayanagi [28] to the case of measuring the distribution of residual stresses in steel bars. Iwayanagi [28] calculated the theoretical relation between stress and magnetization for polycrystalline iron crystals and indicated that the theoretical values agreed well with the experimental values obtained from carbon steels. He also suggested that the magnetic output m would change in a biaxial stress state as $m = A + B (\sigma_1 - 0.5 \sigma_2)$, where σ_1 and σ_2 were the principal stresses in the direction of parallel and perpendicular to the measuring direction, respectively, and A and B were constants. This relation is important because it indicates the possibility of measuring the principal stresses in a biaxial stress state. However, it has not yet been confirmed experimentally. All of these experiments in high fields were performed by using a solenoid coil in which a specimen was inserted. Thus, the methods are not applicable for measuring stresses in steel plates.

To summarize the present situation of the methods for measuring stresses utilizing magnetostriction, it is convenient

to divide the methods into two classes, i.e., the methods in low fields and those in high fields. The main features of the two methods are summarized in Table. 1.1.

TABLE 1.1

SUMMARIZED PRESENT SITUATION OF THE METHODS FOR MEASURING STRESS UTILIZING MAGNETOSTRICTION

Method	Agreement with the theory	Biaxial stress measurement	Influence of material nature***	Probe method
Methods in high fields	Good	Possible*	Small	None
Methods in low fields	Poor	Almost impossible**	Large	Exist

* Theoretically possible but experimentally not confirmed yet.
** Possible for the difference of principal stresses. To separate these principal stresses, the shear difference method is required.
*** e.g. carbon content, plastic deformation, heat treatment.

It can be seen from Table 1.1 that the methods in high fields have many advantages compared with the methods in low fields. However, the methods in high fields involve no probe methods, which are required in a practical usage. The development of a probe method utilizing magnetostriction in high fields therefore has been desired [29].

Under these circumstances, this study aims to develop a probe method utilizing magnetostriction in high fields at the starting point. Chapter II discusses a new kind of magnetic probes which can sense the variation of magnetic permeability

of a steel plate at a high field. Some characteristics of the probes are examined experimentally by using steel plates as specimens. The hysteresis phenomenon in the relationship between stress and the magnetic output of the probe is observed in the experiment and is left to be solved.

Chapter III deals with the hysteresis phenomenon in the relationship between stress and magnetic permeability. A steel bar is used for a specimen, and a solenoid coil is used for producing high fields. Existence of a critical value of the biasing field, under which the hysteresis is observed and over which it is not observed, is demonstrated by the experiment. Theoretical discussions based on the domain theory are also performed and the results are compatible with the experimental results. It is concluded that the stress measured by this method can be determined as a unique value when the magnetizing field is higher than the critical value.

Chapter IV elaborates on a method for measuring stresses based on law of approach to saturation magnetization. The theoretical formula for the measurement of stresses is deduced on the basis of this law. In order to verify the formula, the relationships between stress and permeability are investigated for various specimens of steel rods. The experiments were consistent with the theoretical formulas.

Chapter V validates a probe method based on the theoretical formula described in Chapter IV. It confirms the theory that the probe output has a linear relation with stresses. Biaxial stresses are also measured by the probe using cruciform

specimens, and the results show that the principal stresses can be measured by the method.

Chapter VI summarizes the concluding remarks of this thesis and also mentions the further researches required in this field.

REFERENCES FOR CHAPTER I

[1] Soc. Mat. Sci. Japan, "X-ray stress measurement", p. 1 (1981) Yokendo, Tokyo (in Japanese).

[2] K. Kaneta and H. Nishizawa, Trans. A.I.J., 320, 21 (1982) (in Japanese).

[3] Y. H. Pao, W. Sachse, and H. Fukuoka, Physical Acoustics, **17**, 61 (1984) Academic Press, Orlando.

[4] H. Fukuoka, H. Toda, and H. Naka, Exp. Mech., **23**, 120 (1983).

[5] K. Azumi and J. Iwayanagi, Oyo Buturi, **16**, 179 (1947) (in Japanese).

[6] Y. Osaki, Trans. A.I.J., 40, 40 (1950).

[7] J. Iwayanagi and A. Yoshinaga, Proc. 13th Jpn. Natl. Cong. Appl. Mech., 102 (1963).

[8] A. Yoshinaga, Rep. Ship Res. Inst., **17**, 1 (1980) (in Japanese).

[9] S. Abuku, Jpn. J. Appl. Phys., **16**, 1161 (1977).

[10] R. Langman, IEEE Trans. Magn., **17**, 1159 (1981).

[11] R. Langman, NDT Int., **14**, 255 (1981).

[12] R. Langman, NDT Int., **15**, 91 (1982).

[13] R. Langman, NDT Int., **16**, 59 (1983).

[14] K. Kashiwaya, H. Sakamoto, M. Ito, Y. Ueno, and H. Yamada, Hihakai Kensa, **34**, 201 (1985) (in Japanese).

[15] K. Kashiwaya, H. Sakamoto, and Y. Inoue, Hihakai Kensa, **35**, 519 (1986) (in Japanese).

[16] S. Abuku and T. Isono, Hihakai Kensa, **35**, 805 (1986) (in Japanese).

[17] S. Kishimoto, M. Itoh, H. Yamada, and K. Kashiwaya, Hihakai Kensa, **35**, 861 (1986) (in Japanese).

[18] K. Kashiwaya, H. Sakamoto, and Y. Inoue, Hihakai Kensa, **36**, 894 (1987) (in Japanese).

[19] T. Isono and S. Abuku, Hihakai Kensa, **38**, 253 (1989) (in Japanese).

[20] W. F. Brown, Jr., Phys. Rev., **75**, 147 (1949).

[21] D. J. Craik and M. J. Wood, J. Phys. D: Appl. Phys., **3**, 1009 (1970).

[22] R. R. Birss, IEEE Trans. Magn., **7**, 113 (1971).

[23] D. C. Jiles and D. L. Atherton, J. Phys. D: Appl. Phys., **17**, 1265 (1984).

[24] R. Langman, IEEE Trans. Magn., **21**, 1314 (1985).

[25] J. Iwayanagi and S. Abuku, Proc. 10th Jpn. Cong. Test. Matr., 47 (1967).

[26] J. Iwayanagi and S. Abuku, Proc. 11th Jpn. Cong. Matr. Res., 116 (1968).

[27] S. Abuku and B. D. Cullity, Exp. Mech., **11**, 217 (1971).

[28] J. Iwayanagi, Rep. Ship Res. Inst., **12**, 67 (1975) (in Japanese).

[29] J. Iwayanagi and S. Abuku, Oyo Buturi, **47**, 161 (1978) (in Japanese).

CHAPTER II

MAGNETIC PROBE FOR MEASURING STRESS IN STEEL UTILIZING MAGNETOSTRICTION IN HIGH FIELDS

2.1 INTRODUCTION

There are some types of nondestructive methods for measuring stresses in steel which are based on the inverse magnetostrictive effect (a change in magnetization under applied stresses). It is convenient to divide the methods into two classes: the methods in low magnetic fields and those in high magnetic fields. The methods in low fields correspond to the magnetizing process of the displacement of domain walls (< 1 kA/m for iron), and those in high fields correspond to that of the rotation of magnetization vectors (> 1 kA/m for iron).

As mentioned in the previous chapter, the methods in low fields have some disadvantages especially on the greater influence of the nature of material such as plastic deformation [1], carbon content [2,3], or heat treatment [3] compared with those in high fields. Furthermore, the methods in low fields can not measure the principal stresses of a biaxial state, whereas the methods in high fields can measure them in principle [4]. However, the probe method utilizing magnetostriction in high fields have not been demonstrated yet, while some probe

methods in low fields have already been demonstrated [1-3,5]. In engineering applications where winding a coil around the measuring object is troublesome or impossible, it is highly recommended to develop a probe method utilizing magnetostriction in high fields [6].

In this chapter, a probe method developed for measuring stresses in steel plates is discussed. This is based on the linear dependence of reversible permeability on stresses in high biasing fields [4]. Using steel-plate specimens, some characteristics of the probe were examined experimentally and the results were compared with the theoretical values derived from the domain theory. The measurements in the direction parallel and perpendicular to applied stresses were also carried out to examine the possibility for measuring the principal stresses in a biaxial state.

2.2 EXPERIMENTAL PROCEDURE

2.2.1 Specimen

The specimens used were hot-rolled carbon steel plates of SS41 in Japan Industrial Standard (JIS), and their thickness was 3.2 mm. The chemical compositions in weight percentage are shown in Table 2.1. Two types of specimens were used for tension: one had a narrow width of 20 mm and the other had a wide width of 90 mm. They will be called Narrow specimen and Wide specimen, respectively. The machined specimens were annealed to reduce residual stresses at 650°C for one hour in vacuum and cooled naturally in the furnace.

TABLE 2.1

CHEMICAL COMPOSITIONS OF THE MATERIAL USED (SS41) IN WEIGHT %

C	Si	Mn	P	S
0.11	0.007	1.08	0.013	0.006

2.2.2 Apparatus

Two types of probes were used: Probe 1 for Narrow specimen and Probe 2 for Wide specimen.

Figure 2.1 shows the measuring setup and the magnetic probe used for the measurement of Narrow specimen (Probe 1). The probe consists of a probe yoke, three coils wound on the yoke, and a Hall sensor attached on the surface of the specimen.

The probe yoke was machined from the lamination of silicon steel plates whose thickness is 0.5 mm to the shape shown in Fig. 2.1. If the probe yoke is saturated magnetically before the specimen is saturated, the magnetic flux can not flow any more in the magnetic circuit which consists of the probe yoke and the specimen, and the fields in the specimen will be saturated at the value of saturation of the probe yoke. On the contrary, when the saturation of the specimen precedes that of the probe yoke, the fields in the specimen increase almost proportionately to the magnetizing current. The capacity of the flux flow in the probe yoke should, therefore, be more than that in the specimen in order to produce high fields in the specimen. Because the saturation flux of Narrow specimen was

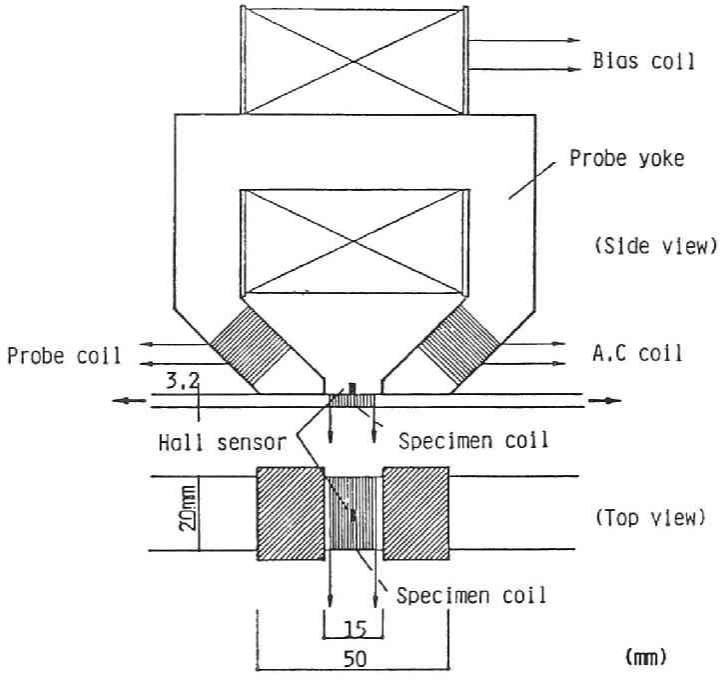

Fig. 2.1 Measuring setup and magnetic probe used for the measurement of Narrow specimen (Probe 1).

around 0.14 mWb, the probe yoke should be designed to have the saturation flux above this unit. In this case, the saturation flux of the probe yoke was designed to have 0.60 mWb.

The direct current in the bias coil produces flux through the yoke and the specimen. The flux in turn induces the biasing fields in the specimen. The strength of the biasing field is measured by the Hall sensor attached on the specimen surface. Because the parallel component of the field strength to the specimen surface in air has the same value as that in the specimen, the field strength measured by the Hall sensor on the specimen surface indicates that in the specimen.

The relationship between the field strength H at the center of the gap of the probe legs and the magnetizing current I can be expressed by the following formula:

$$H = nI/l \qquad (2.1)$$

where n is the turn number of the bias coil and l is the distance between the two magnetic poles caused by flux flow on the specimen. Letting l = 15 mm and n = 523, the formula become H = 34.9I kA/m. The empirical formula was obtained as H = 28.7I kA/m, in which the magnitude of the coefficient was somewhat smaller than that for the theoretical formula. From the empirical formula, l was calculated as 18 mm. The lengthening of l may be produced by saturation of the probe yoke at its pointed ends.

Around both legs of the probe, coils are wound: one is

named A. C. coil, along which alternative current passes, and the other is named Probe coil, in which alternative voltage is induced by alternative flux through the yoke. The alternative current used in the experiment had a frequency of 1 kHz. The alternative field strength caused by the current in the specimen was measured by the Hall sensor whose output voltage was detected with the usage of a lock-in amplifier (NF LI-570). This alternative field strength was adjusted to the value of 80 A/m (in r.m.s.) by controlling the magnitude of the alternative current. The alternative flux was also measured by using a lock-in amplifier from the voltage induced in the probe coil. For the reference, Specimen coil was also wound around the specimen at the gap of the legs of the probe yoke.

Because the ratio of flux to field strength equals the product of permeability and the sectional area in which flux flows, the following formula can be deduced:

$$\mu_{rev}S = \phi/(\mu_0 h) \qquad (2.2)$$

where μ_{rev} is the reversible relative permeability, S is the sectional area in which the alternative flux flows, ϕ is the alternative flux, h is the alternative field strength, and μ_0 is the permeability of free space ($4\pi \times 10^{-7}$ H/m). $\mu_{rev}S$ has a dimension of square meter. Hereafter, $\mu_{rev}S$ will be referred to as the magnetic output.

Probe 2 consists of the same components as Probe 1, but the probe yoke is split into three pieces as shown in Fig. 2.2.

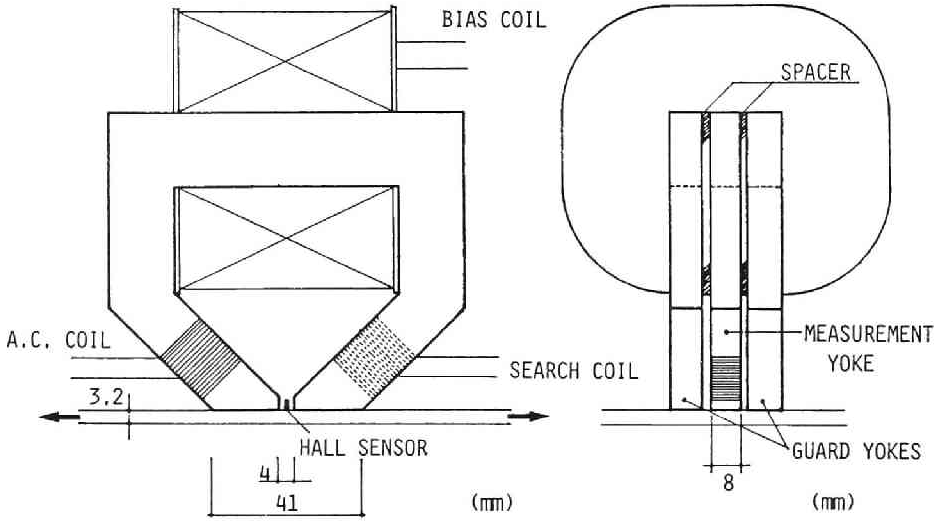

Fig. 2.2 Measuring setup and magnetic probe used for the measurement of Wide specimen (Probe 2).

A. C. coil is wound around one leg of the yoke over three pieces, and Search coil is wound only around the central piece of the other leg. Note that Probe 2 had no Specimen coil. The two outer yokes limit the flux flow of the central magnet circuit; this "guard yoke system" has been demonstrated by Wilkins and Drake [7,8] and Langman [9]. Only the flux whose direction is parallel to the measuring direction will be detected with the use of this guard yoke system.

2.3 EXPERIMENTAL RESULTS

2.3.1 Depth of the Measured Area

The field strengths on the surface of each side of the specimens were measured by using the Hall sensor. The field strength on the specimen surface on which the magnetic probe was attached was defined as H_0 or h_0, and that on the back surface was defined as H_t or h_t, where the capital letter and the small letter represented the biasing field and the alternative field, respectively. Because the sensitive point of the Hall sensor (whose sensitive area was under 0.1 mm^2) was 1.5 mm far from its edge, the field strengths on the surface were determined by extrapolating linearly from the measured values along the vertical direction to the specimen surface. Narrow specimen was used for the measurement by Probe 1, and Narrowed specimen, which is shown in Sec. 2.3.3, was used for the measurement by Probe 2.

Figure 2.3 shows the relative field amplitude H_t/H_0 and h_t/h_0 as a function of the biasing fields. The relative

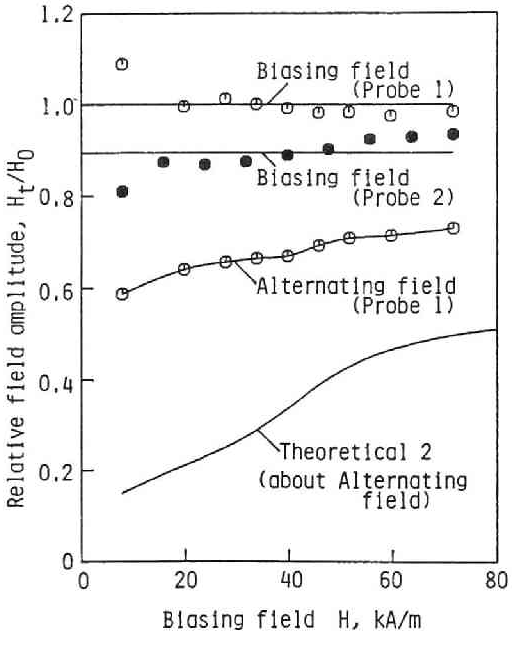

Fig. 2.3 Relative field amplitude as a function of biasing field.

amplitude of the biasing fields H_t/H_0 for Probe 1 has the average value of 1.0, so the biasing fields are distributed uniformly through the thickness of the specimen. Probe 2, however, has the average biasing field value of 0.9, 10 percent lower from the surface of the probe side to that of the back side. The relative amplitude of the alternative fields h_t/h_0 was measured for Probe 1. As shown in Fig. 2.3, h_t/h_0 increases as the biasing field increases. In other words, the penetration depth of the alternative fields increases as the biasing field increases. The average of h_t/h_0 is about 0.7, which means that the stresses measured by this method is approximate to the averaged stresses throughout the thickness of the specimen. The theoretical curve drawn in Fig. 2.3 is explained in Sec. 2.4.

2.3.2 Stress Dependence of Narrow Specimen

While tensile stress was applied to and removed from Narrow specimen under the constant biasing fields, the magnetic outputs of Probe 1 were measured. When the stress varied, the value of the biasing field also varied under a constant magnetizing current. Thus the adjustment of the magnetizing current was required to keep constant the biasing field. The adjustment of the alternative magnetizing current, however, was not carried out because a minimal change of the alternative field strength did not alter the magnetic output. The measurements were performed under the biasing fields up to 72 kA/m.

Figure 2.4 shows an example of the variation of the magnetic

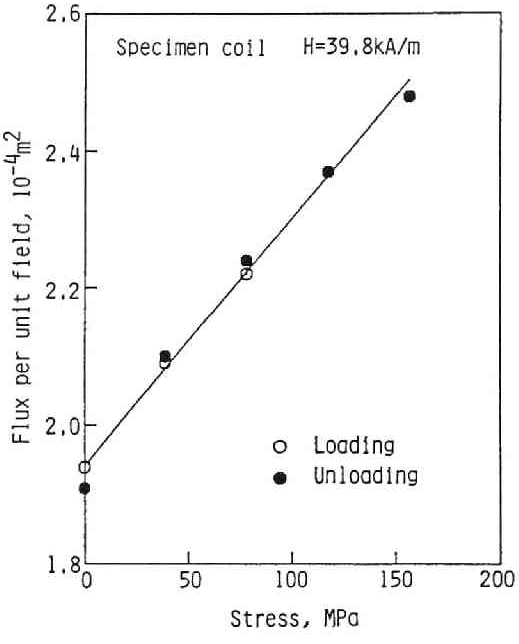

Fig. 2.4 Variation of the magnetic output of Probe 1 with tensile stress.

output of Probe 1 with tensile stress for Narrow specimen. The relation between the stress and the variation of the magnetic output is almost linear. The linear relation was observed for both Probe coil and Specimen coil. Thus the experimental results can be expressed as follows:

$$\mu_{rev}S = (\mu_{rev}S)_0 + \Lambda_{rev}S\ \sigma \qquad (2.3)$$

where $(\mu_{rev}S)_0$ and $\Lambda_{rev}S$ are named the initial value and the stress sensitivity, respectively.

The initial value and the stress sensitivity as a function of the biasing field are shown in Figs. 2.5 and 2.6, respectively. The initial value decreases as the biasing field increases. The initial value for Probe coil is larger than that for Specimen coil. The stress sensitivity has a peak at around 40 kA/m of the biasing field for both Specimen coil and Probe coil.

The difference between the magnetic output of Probe coil and that of Specimen coil is due to the flux that fringes through the air. As a result, the relative stress-sensitivity for Probe coil is reduced in comparison with that for Specimen coil; however, it has still high value, i.e., 0.35 GPa^{-1} at the maximum. The uniaxial tensile stress, therefore, can be measured for an object whose width is the same as that of the probe yoke by using this kind of method.

2.3.3 Stress Dependence of Wide Specimen

As shown in Fig. 2.7, the measurement of Wide specimen

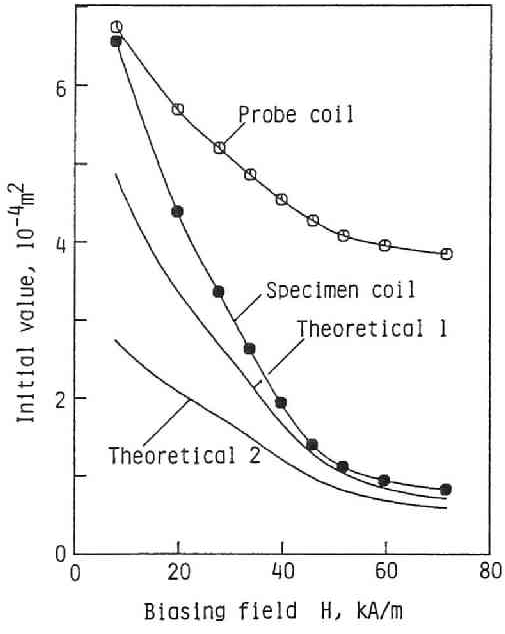

Fig. 2.5 Initial value for Probe 1 as a function of biasing field.

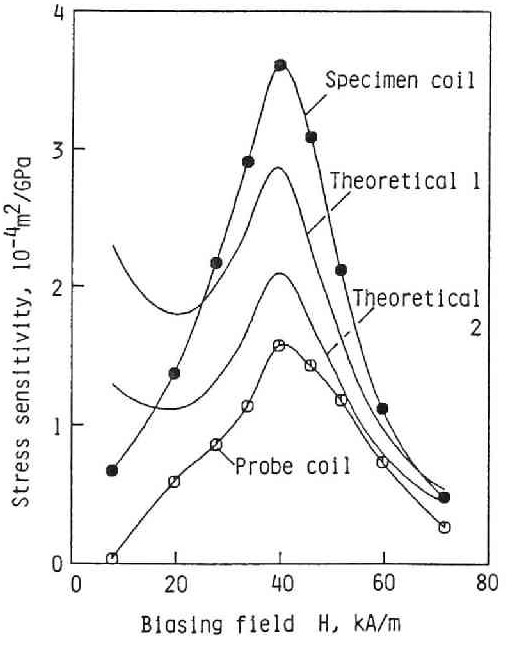

Fig. 2.6 Stress sensitivity for Probe 1 as a function of biasing field.

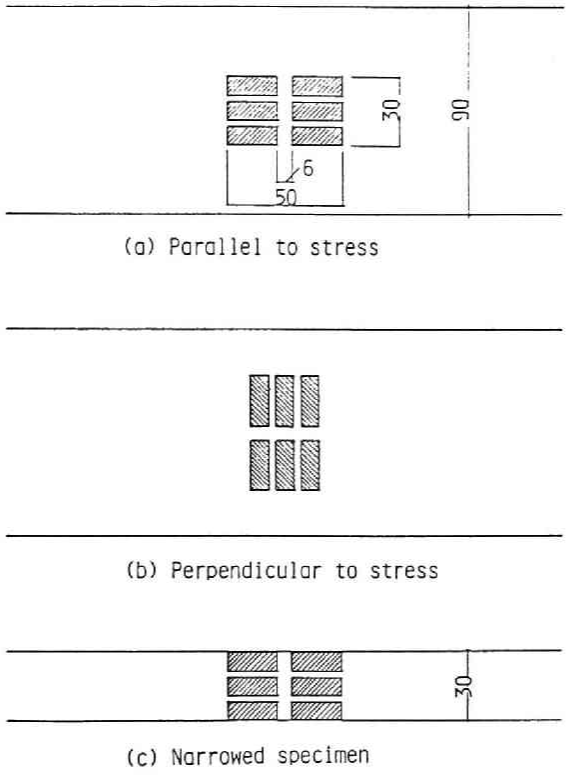

Fig. 2.7 Setup for the measurement of Wide specimen by Probe 2.

was performed in the direction parallel and perpendicular to the tension by using Probe 2. After the measurement, Wide specimen was cut into a width of 30 mm (Narrowed specimen), and the magnetic outputs in the direction parallel to the tension were measured. The measuring conditions were the same as those for Narrow specimen. However, the measurement for Wide specimen was performed only at the biasing fields up to 50 kA/m, which was the maximum obtained due to the magnetic saturation of the probe yoke.

Figure 2.8 shows an example of the variation of the magnetic output with tensile stresses in the direction parallel to the tension for Wide specimen. Hysteresis of the magnetic output due to the applied stress, where only the first loading curve is different from the subsequent unloading curve and the curves after that, can be seen. However, in the direction perpendicular to the tension, the hysteresis was not remarkably observed as that in the parallel direction. The variation of the magnetic output for Narrowed specimen did not indicate the hysteresis phenomenon in the same manner as Narrow specimen.

The linear relation was found between the applied stress and the magnetic output except for the first loading curve. The initial value and the stress sensitivity for the second loading and unloading curves as a function of the biasing field are shown in Figs. 2.9 and 2.10, respectively. The initial values decrease as the biasing field increases, similar to Narrow specimen. The stress sensitivity for Narrowed specimen has its peak at around H ≈ 43 kA/m. After the correction for the

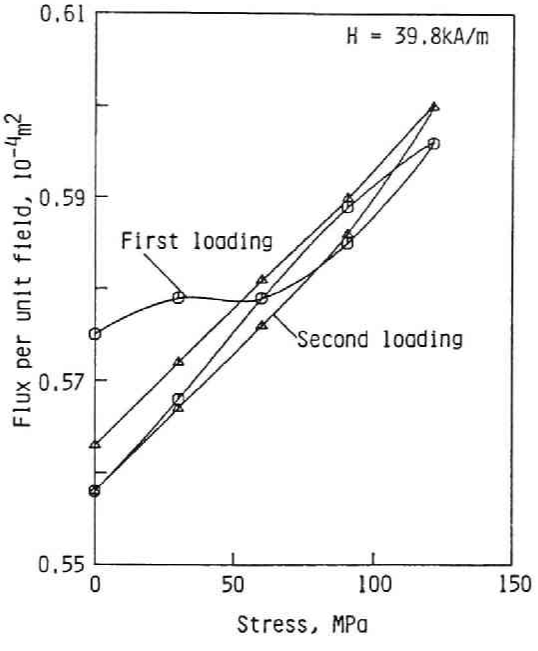

Fig. 2.8 Variation of the magnetic output of Probe 2 to the tensile stress. Measured in the direction parallel to the stress for Wide specimen.

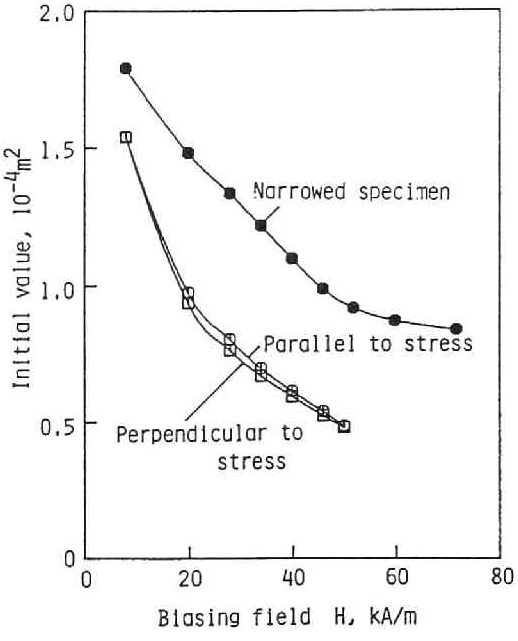

Fig. 2.9 Initial value for Probe 2 as a function of biasing field.

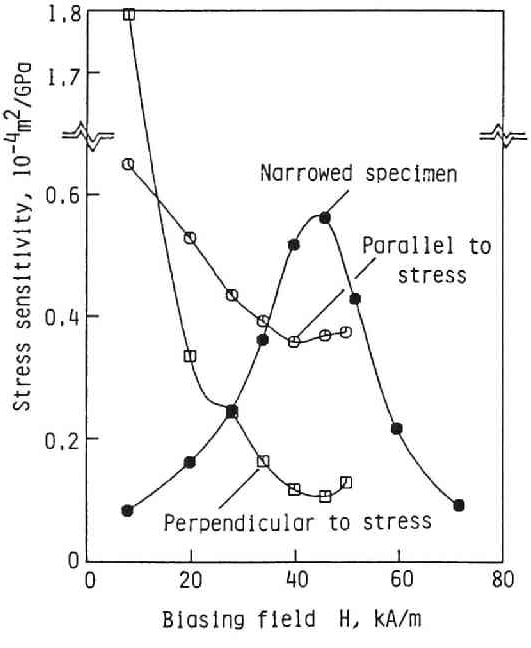

Fig. 2.10 Stress sensitivity for Probe 2 as a function of biasing field.

reduction of the biasing field through the thickness of the specimen, the peak point, 43 kA/m, is reduced to around 41 kA/m. Therefore, the peak point agrees with that for Narrow specimen. These results indicate that Probe 2 has the same characteristics as Probe 1 in its basic feature, i.e., the linear relation between the applied stress and the magnetic output, and the peak of the stress sensitivity at H = 40 kA/m.

The stress sensitivity for Wide specimen in the direction both parallel and perpendicular to the tension dose not peak at around H = 40 kA/m, and the curves are far different from those of Narrowed specimen. In addition, the ratio of the stress sensitivity perpendicular to the tension compared to that parallel to the tension disagrees with the theoretical value of -0.5, which was indicated by Iwayanagi [4].

2.4 DISCUSSION

Iwayanagi [4] calculated the reversible permeability of iron as a function of the biasing field and the applied stress on the basis of the domain theory. He expressed reversible permeability μ_{rev} as a linear function of stress σ as follows:

$$\mu_{rev} = \mu_{rev0} + \Lambda_{rev}\,\sigma \qquad (2.4)$$

where μ_{rev0} represented the initial value and Λ_{rev} represented the stress sensitivity. Both μ_{rev0} and Λ_{rev} are functions of the biasing fields. The theoretical values are tabulated in Table 2.2.

TABLE 2.2

THEORETICAL VALUES OF μ_{rev0} AND Λ_{rev}

H (kA/m)	8.0	15.9	23.9	31.8	39.8	47.7	55.7	63.7	71.6
μ_{rev0}	9.79	7.47	5.88	4.56	3.23	2.25	1.74	1.48	1.33
Λ_{rev} (GPa^{-1})	4.60	3.70	3.57	4.35	5.50	3.90	2.34	1.48	1.01

When the applied field is alternative, the field strength at the point of the depth t from the surface is given by the following formulas:

$$h_t/h_0 = \exp(-t/\delta) \tag{2.5}$$

$$\delta = \left(\frac{\rho}{\pi f \mu}\right)^{1/2} \tag{2.6}$$

where ρ is the resistivity, f is the frequency of the alternative field, μ is the magnetic permeability, and δ is the skin thickness [10]. At the depth δ below the surface, the field strength is the 1/e-th of that at the surface.

The theoretical values of h_t/h_0 were calculated with μ_{rev0} given in Table 2.2 and the resistivity of ρ = 0.1 $\mu\Omega$m, which is the standard value of iron. They are drawn in Fig. 2.3. The theoretical value increases as the biasing field increases in the same manner as the experimental curve. However, the theoretical value is considerably smaller than the experimental value. In other words, the penetration of the alternative fields

is much deeper than the theoretical prediction. Although the reason is not clear, it may be due to the flux that fringes through the air.

Theoretical values of $(\mu_{rev}S)_0$ and $\Lambda_{rev}S$ were calculated by two different ways; they are given as theoretical 1 and theoretical 2, respectively. They are different in the estimation of the measured area S. Theoretical 1 was calculated by using the experimental data of h_t/h_0 where the distribution of the fields was assumed as linear; on the other hand, theoretical 2 was calculated from the theoretical distribution of the fields given by eqs. (2.5) and (2.6). These values are shown in Figs. 2.5 and 2.6. The experimental values for Specimen coil concurred with the values of theoretical 1. On the other hand, experimental values for Probe coil differed from the theoretical values, but the peak point of the stress sensitivity, i.e., H = 40 kA/m, was consonant with the theoretical prediction. In conclusion, at least qualitatively, the magnetic outputs agree well with the theoretical predictions derived from the domain theory when the width of the specimen is the same as that of probe.

However, the conclusion for Narrow specimen is not applicable to Wide specimen due to the following problems:

(1) Hysteresis of the magnetic output due to stress.

(2) Disagreement of the stress sensitivity with the theory.

The two problems may be related closely or may be independent of each other. The second problem may not be significant because calibration tests can be carried out experimentally. The first

problem--hysteresis due to stress--is, however, more significant because the stress can not be determined as a unique value with this measurement. Therefore, the hysteresis problem must be solved.

2.5 CONCLUSIONS

A new kind of magnetic probes which can sense the variation of permeability of a steel plate at a high magnetic field was discussed. The results obtained are summarized as follows:

(1) When the width of a specimen was the same as that of the probe, the magnetic outputs of the probe varied linearly with applied tension as the theory predicted. In this case, the experimental values of the initial value and the stress sensitivity were compatible, at least qualitatively, with the theoretical predictions derived from the domain theory.

(2) When the width of a specimen was wider than that of the probe, the magnetic outputs were far different from the theoretical predictions, and hysteresis due to applied tension was observed.

In conclusion, the application of the method described in this chapter is limited to an object whose width is the same as that of the probe. Otherwise, if the width of an object is wider then the probe, the hysteresis problem arises and this must be solved.

REFERENCES FOR CHAPTER II

[1] S. Abuku, Jpn. J. Appl. Phys., **16**, 1161 (1977).

[2] J. Iwayanagi and A. Yoshinaga, Proc. 13th Jpn. Natl. Cong. Appl. Mech., 102 (1963).

[3] A. Yoshinaga, Rep. Ship Res. Inst., **17**, 1 (1980) (in Japanese).

[4] J. Iwayanagi, Rep. Ship Res. Inst., **12**, 67 (1975) (in Japanese).

[5] R. Langman, NDT Int., **16**, 59 (1983).

[6] J. Iwayanagi and S. Abuku, Oyo Buturi, **47**, 161 (1978) (in Japanese).

[7] F. J. Wilkins and A. E. Drake, Proc. Inst. Electr. Eng., **112**, 786 (1965).

[8] F. J. Wilkins and A. E. Drake, Proc. Inst. Electr. Eng., **117**, 1048 (1970).

[9] R. Langman, NDT Int., **14**, 255 (1981).

[10] R. M. Bozorth, "Ferromagnetism", p. 771 (1951) D. Van Nostrand Co., Princeton.

CHAPTER III

CRITICAL FIELD ON HYSTERESIS OF MAGNETIZATION DUE TO STRESS

3.1 INTRODUCTION

The hysteresis phenomenon of magnetization due to stress, which was observed in the previous chapter, is a significant problem for stress measurement because the stress measured by this magnetic method can not be determined as a unique value. In this chapter, this hysteresis phenomenon is examined experimentally and a theoretical model is proposed on the basis of the domain theory.

Iwayanagi and Abuku [1] reported a load cell which is based on the linear relation between reversible permeability and stress under biasing field. They observed the same hysteresis phenomenon as shown in the previous chapter, i.e., only the first loading cycle differed from the cycles succeeding the first one. They indicated that the hysteresis error was much reduced when the biasing field was not shut off and the succeeding cycles were kept. Thus, they used a permanent magnet to supply biasing fields and reduced the hysteresis phenomenon. Unfortunately, we could not use this technique for stress measurement because we could not apply stresses to the measuring

object and thus we could not measure the reversible permeability on the succeeding cycles. In addition, the nature of the hysteresis due to stress has not been clarified. It is, therefore, necessary to clarify the nature of the hysteresis first in order to solve the hysteresis problem.

It is known that the hysteresis error decreases with an increase of the field strength applied to the specimen [1]. The variation of the hysteresis error with biasing field strength was therefore examined experimentally. Because the state of residual magnetization affects the hysteresis error, this should be restrained. For this purpose, high biasing field of 79.6 kA/m, which align the magnetization vectors along the longitudinal direction of the specimen, was applied before the measurement. The experimental results indicated that a critical value of around 45 kA/m of the biasing field existed, under which the hysteresis was observed and over which it was not observed.

The magnetization process of low-carbon steels in low and moderate fields may be explained satisfactorily by the Becker-Kersten treatment of domain boundary movement. However, it seems improbable to account for high value (45 kA/m) of the critical field solely by the Becker-Kersten treatment. On the other hand, Stoner and Wohlfarth [2] proposed a theoretical model of the magnetic hysteresis of single-domain particles and accounted satisfactorily for higher coercivities which could not be explained by the Becker-Kersten treatment. In this chapter, the same theoretical concept as [2] was applied to

account for the critical field on hysteresis of magnetization due to stress in high fields.

3.2 EXPERIMENTAL PROCEDURE

3.2.1 Specimen

The specimen used was a cold drawn rod of carbon steel of SS41 in JIS-code. It had a length of 900 mm and a diameter of 10 mm, and was annealed to reduce the residual stresses at 650°C for 90 minutes in vacuum and cooled naturally in the furnace. The chemical compositions are shown in Table 3.1. Table 3.2 illustrates the mechanical properties and the resistivity of the specimen. The value of the resistivity was measured by using a double bridge (Yokogawa 2752).

TABLE 3.1

CHEMICAL COMPOSITIONS OF THE USED MATERIAL (SS41) IN WEIGHT %

C	Si	Mn	P	S
0.18	0.27	1.08	0.014	0.016

TABLE 3.2

MECHANICAL PROPERTIES AND RESISTIVITY
OF THE USED SPECIMEN

Tensile strength	Yield strength	Rockwell hardness	Resistivity
MPa	MPa		μΩm
450	278	70(B)	0.190

3.2.2 Measuring Setup

The measuring setup used in this experiment is shown in Fig. 3.1. The outer coil called the D.C. coil supplies the biasing fields to the specimen inserted in the coils. The inductance L of the inner coil termed the A.C. coil is measured by using an impedance analyzer (YHP 4192A). The main feature of this setup has already been demonstrated [3,4].

The coil constant of D.C. coil is 1.46×10^4 m^{-1}, and the distribution of the fields is almost uniform (the decrease of field at the point of 50 mm far from the center along the axis of the coil is 3.2% of the field at the center). The turn number of A.C. coil is 830, the length is 100 mm, and the diameter is 12.88 mm. The measured value of the inductance in air is 1.064 mH, which agrees well with the calculated value of 1.069 mH.

This setup can measure the reversible permeability of the specimen under a biasing field. The procedure to determine the reversible permeability μ_{rev} from the measured value of the inductance L is summarized in Appendix.

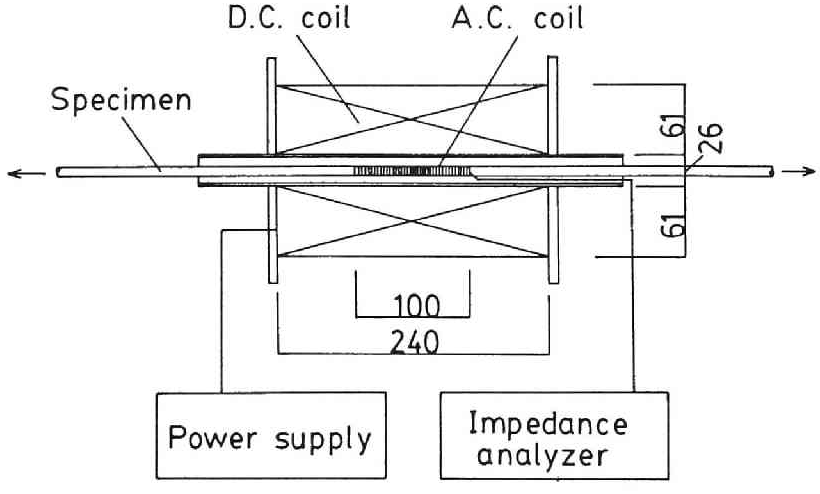

Fig. 3.1 Setup for the measurement of reversible permeability of specimen under applied stress.

The frequency for the measurement of the inductance is 1020 Hz, and the amplitude of the alternative fields is around 40 A/m. Because the typical value of the reversible permeability in this experiment is 2, skin thickness δ has the value around 5 mm. This means that the magnitude of the field at the center of the specimen is 1/e-th of that of the field at the surface of the specimen.

Both ends of the specimen were fixed to the loading jig of steel to reduce the demagnetizing fields. The resulting demagnetizing factor is, thus, very small (under 10^{-4}) in such a way that the values of both biasing field and reversible permeability were not corrected for demagnetizing effects.

3.2.3 Measuring procedure of reversible permeability

Figure 3.2 shows a schematic representation of the hysteresis loop, which indicates the relation between the magnetic inductions B and the magnetizing fields H. In this experiment, the reversible permeabilities were measured on the curves both a-b and b-c. Because the reversible permeability on the curve a-b can give the maximum value of the reversible permeabilities measured under the biasing field, it is represented here by the symbol μ_{max}. On the other hand, because the reversible permeability on the curve b-c can give the minimum value of the reversible permeabilities measured under the biasing field, it is represented here by the symbol μ_{min}.

μ_{max} was measured by the following procedure: First, applying the biasing field of -79.6 kA/m (a negative sign

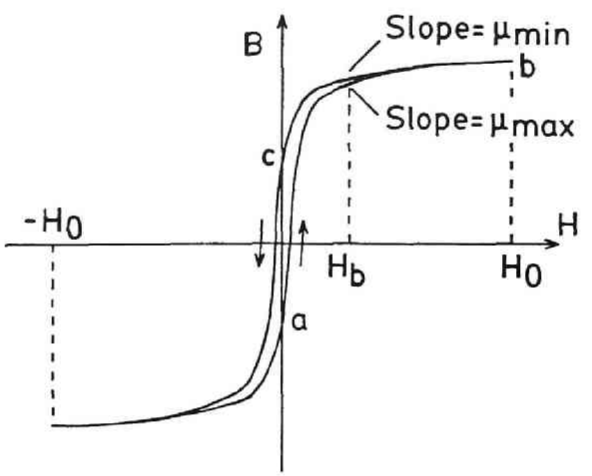

Fig. 3.2 Schematic representation of the hysteresis loop. μ_{max} is defined as the reversible permeability on the curve a-b and μ_{min} is defined on b-c. H_b represents the biasing field under which the measurements are made. H_0 is 79.6 kA/m in this experiment.

indicates that the direction of the field is opposite to the direction of the field under the measurement of μ_{rev}) to the specimen, second, increasing the biasing field up to the set point H, third, measuring the inductance of A.C. coil, last, calculating μ_{max} from the measured value of the inductance.

μ_{min} was measured by the following procedure: First, applying the biasing field of 79.6 kA/m to the specimen, second, decreasing the biasing field up to the set point H, third, measuring the inductance of A.C. coil, last, calculating μ_{min}.

Because the biasing fields of the magnitude of 79.6 kA/m can align the magnetization vectors to the same direction as the biasing fields applied, the state of the residual magnetization does not affect the measurement. At the same time, μ_{max} and μ_{min} can give both ends of the reversible permeability under the biasing field, in order to determine whether the reversible permeability has a unique value or not under the biasing field.

3.3 EXPERIMENTAL RESULTS

3.3.1 Effect of the Setting Speed of Biasing Fields

Figure 3.3 shows the effect of the setting (increasing or decreasing) speed of biasing fields on the difference of reversible permeabilities $\mu_{max} - \mu_{min}$. In Fig. 3.3, the setting speed is plotted in the dimension of its inverse, i.e., the setting time. When the setting speed is fast, $\mu_{max} - \mu_{min}$ has a negative value, which disagrees with the hypothesis that μ_{max} and μ_{min} give the maximum and the minimum of the reversible permeabilities, respectively, under the biasing field. On the

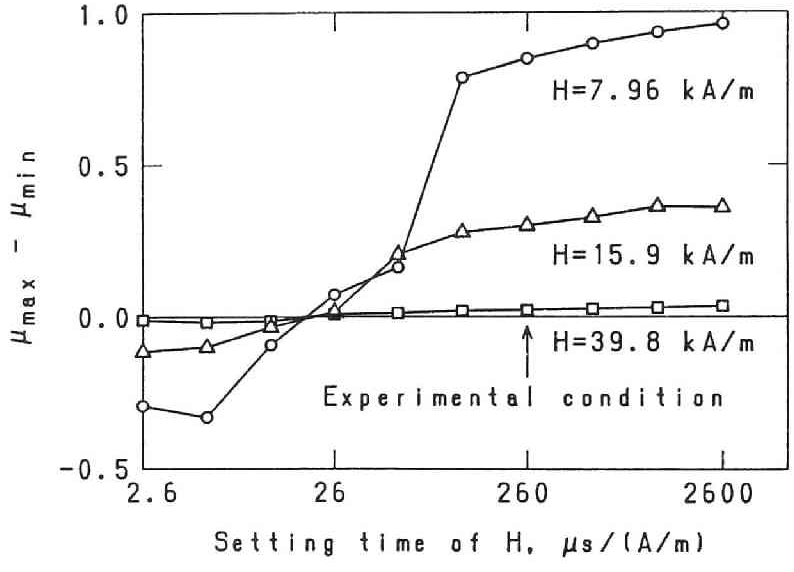

Fig. 3.3 Effect of the setting speed of biasing fields H on the difference of reversible permeabilities $\mu_{max} - \mu_{min}$. In this figure, the setting speed is plotted in the dimension of its inverse, i.e., the setting time.

other hand, when the setting speed is slow, $\mu_{max} - \mu_{min}$ has a positive value, which agrees with the hypothesis. It can also be seen that when the setting time is longer than the critical value of 130 μs/(A/m), the values $\mu_{max} - \mu_{min}$ become almost constant. The value of 260 μs/(A/m) was thus chosen as the setting time in this experiment. The nature of this effect may relate to the dynamic behavior of the domain walls and/or the rotation of the magnetization vectors. This phenomenon is interesting; however, further discussion is limited since it is not within the scope of this paper.

3.3.2 Relation between Reversible Permeability and Stress

The reversible permeabilities μ_{max} and μ_{min} were measured at the constant biasing field H under applied stresses. The experiment were carried out for the biasing fields from 7.96 kA/m to 79.6 kA/m. Figure 3.4 shows the example of the obtained curves.

Figure 3.4 (a) for H = 7.96 kA/m indicates that the values of μ_{max} and μ_{min} are much different. The hysteresis phenomenon where the first loading curve differs from the unloading curve and the curves after that can also be seen for both μ_{max} and μ_{min}. The first loading curve is larger than the other curves for μ_{max}; on the other hand, the first loading curve is smaller than the other curves for μ_{min}. The same feature was obtained in the results for H = 15.9 kA/m.

Figure 3.4 (b) for H = 23.9 kA/m indicates that the values of μ_{max} and μ_{min} are different in the same way as the case for

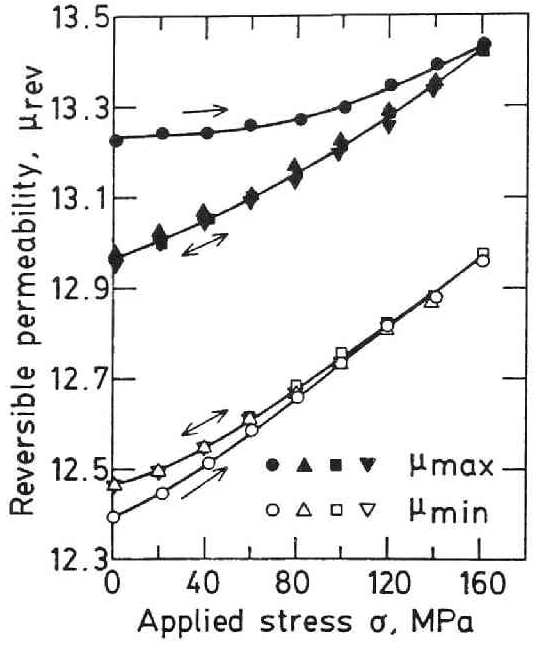

(a) H = 7.96 kA/m.

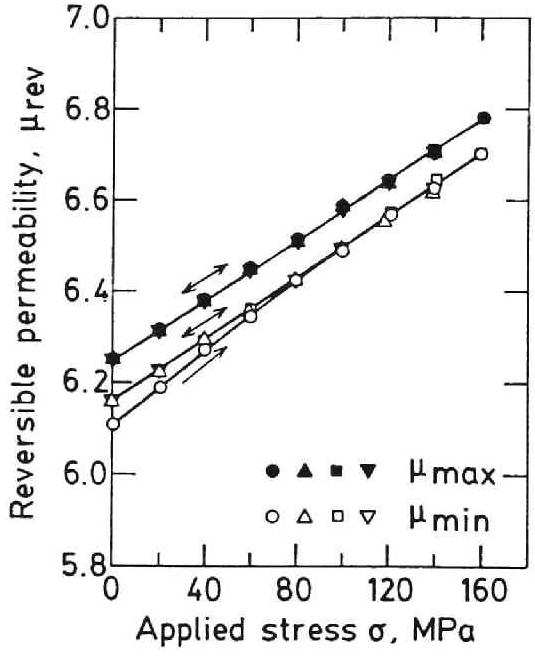

(b) H = 23.9 kA/m.

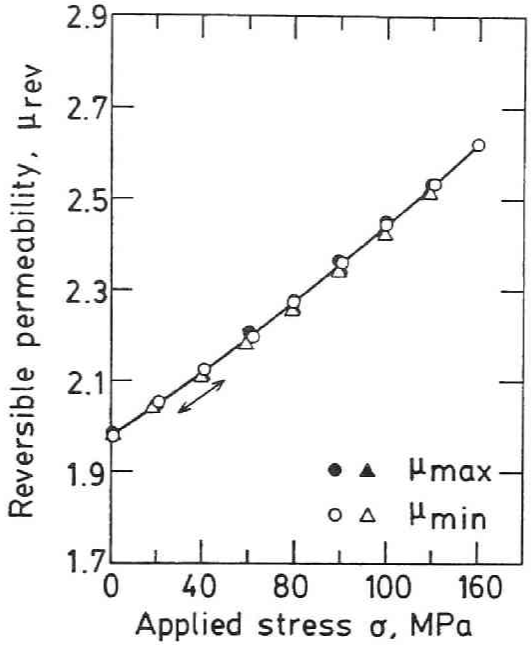

(c) H = 47.8 kA/m.

Fig. 3.4 Variation of the reversible permeabilities with applied stress. The symbols of circle, triangle, square, and inverted triangle indicate first loading, first unloading, second loading, and second unloading curves, respectively.

H = 7.96 kA/m, but the difference is smaller than that for H = 7.96 kA/m. The hysteresis phenomenon is observed for μ_{min}, but it is not observed for μ_{max}. The same feature was obtained in the results for both H = 31.8 kA/m and H = 39.8 kA/m.

Figure 3.4 (c) for H = 47.8 kA/m indicates that the values of μ_{max} agree with those of μ_{min} within the precision of the measurements. Further, the hysteresis phenomenon can not be seen. The same feature was obtained in the results for H = 55.7 kA/m and more. Therefore, when the biasing field is 47.8 kA/m or more, the reversible permeability μ_{rev} can be obtained as a unique value.

Figure 3.5 shows the relationship between $\mu_{max} - \mu_{min}$ and the biasing fields H at the applied stress $\sigma = 0$. It can be noted that the magnitude $\mu_{max} - \mu_{min}$ decreases as the biasing field increases, and it becomes zero at H = 47.8 kA/m and more.

Figure 3.6 shows the relationship between the hysteresis error $\Delta\mu_{rev}$ at $\sigma = 0$ and the biasing fields H. The absolute values of $\Delta\mu_{rev}$ for both μ_{max} and μ_{min} decrease as the biasing field increases. The values of $\Delta\mu_{rev}$ for μ_{max} agree with zero at H = 23.9 kA/m and more, and those for μ_{min} agree with zero at H = 47.8 kA/m and more within the precision of the measurement.

3.4 DISCUSSION

The magnetization process in low and moderate fields is caused mainly by the domain wall movement, and may be explained satisfactorily by the Becker-Kersten treatment. However, it

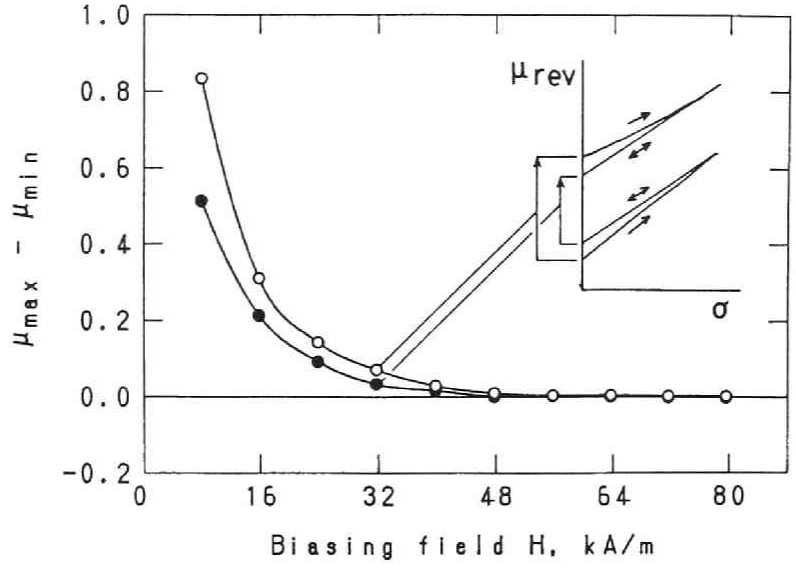

Fig. 3.5 Relationship between $\mu_{max} - \mu_{min}$ at the applied stress $\sigma = 0$ and the biasing fields H.

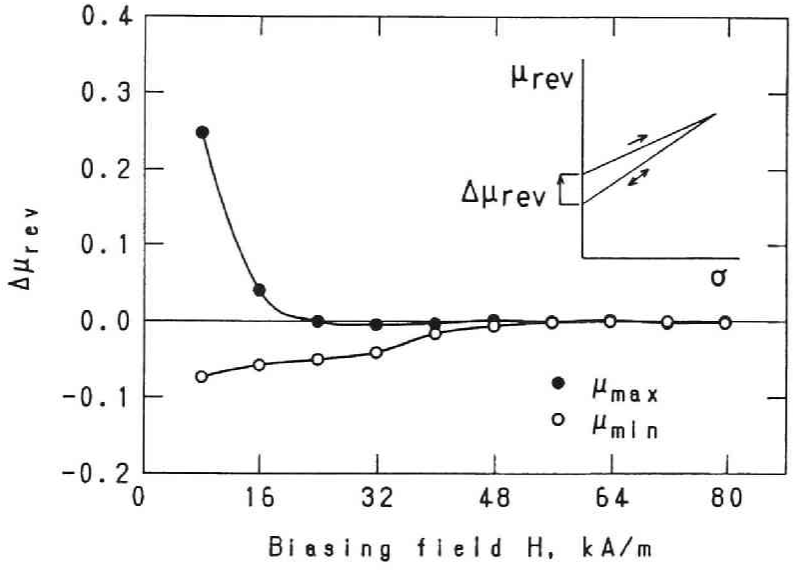

Fig. 3.6 Relationship between $\Delta\mu_{rev}$ at $\sigma = 0$ and the biasing fields H.

seems improbable that higher value of the critical field (around 45 kA/m) is explained solely by the Becker-Kersten treatment because the process of domain wall displacement has probably finished at a moderate field much lower than 45 kA/m.

On the other hand, Stoner and Wohlfarth [2] discussed the nature of the hysteresis of single-domain particles wherein the energy were determined by the shape anisotropy, based on the irreversible rotation of magnetization vectors. Of course, their theory can not apply directly to the case in this experiment because the domain boundary necessarily exist in a low-carbon steel. However, when the domain boundary can not move because of high restriction, we may estimate the irreversible magnetic process by the irreversible rotation of magnetization vectors. In this section, therefore, we assume that the domain boundary can not move, and we apply the the same concept as [2] to account for the critical field of magnetization due to stress.

3.4.1 Discontinuous Rotation of Magnetization Vectors

In general, the direction of magnetization vectors can be determined by minimizing the total energy of the crystals. In high fields where the magnetization process is caused by the rotation of magnetization vectors, the total energy E consists of the energy associated with the applied field E_H, the energy associated with the magneto-crystalline anisotropy E_K, and the energy associated with the strain anisotropy E_σ. Each of them is given in the following [5]:

$$E = E_K + E_H + E_\sigma \tag{3.1}$$

$$E_K = K(\alpha_1^2\alpha_2^2 + \alpha_2^2\alpha_3^2 + \alpha_3^2\alpha_1^2) \tag{3.2}$$

$$E_H = - H I_s \cos \phi \tag{3.3}$$

$$E_\sigma = - (3/2)\sigma [\lambda_{100}(\alpha_1^2\beta_1^2 + \alpha_2^2\beta_2^2 + \alpha_3^2\beta_3^2) + 2\lambda_{111} (\alpha_1\alpha_2\beta_1\beta_2 + \alpha_2\alpha_3\beta_2\beta_3 + \alpha_3\alpha_1\beta_3\beta_1)] \tag{3.4}$$

where H is the applied field, I_s is the magnetization vector, ϕ is the angle between the directions of H and I_s, K is the cubic anisotropy constant, λ_{100} and λ_{111} are the magnetostriction constants, σ is the stress applied in the direction of H, and α_i and β_i (i = 1, 2, 3) are the direction cosines, relative to the crystal axes, of the magnetization vector and the applied field, respectively. The standard values of the constants are I_s = 2.12 T [6], K = 47.2 kJ/m^3 [7], $\lambda_{100} = 20.7\times10^{-6}$, and $\lambda_{111} = -21.2\times10^{-6}$ [8], respectively.

It is complicated and difficult to treat the total energy E in this form. Therefore, we now assume that the vectors of H and σ lie in a (100) plane of an iron-like crystal (K>0). It is clear that the equilibrium directions of magnetization lie in the same plane. The analytical model and the definition of the angles are shown in Fig. 3.7. In this plane, let θ be the angle between the positive direction of H and an easy magnetization axis [100], ϕ the angle between H and I_s, and ψ the angle between the easy axis and I_s. Thus,

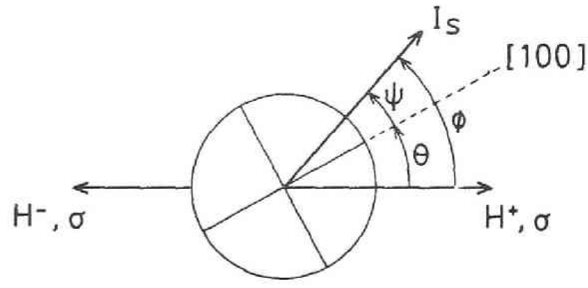

Fig. 3.7 The analytical model and the definition of the angles θ, φ, and ψ in a (100) plane of an iron-like crystal.

$$\phi = \theta + \psi. \tag{3.5}$$

The resolved magnetization I in the direction of H is

$$I = I_s \cos \phi. \tag{3.6}$$

Letting $\alpha = (\cos \psi, \sin \psi, 0)$ and $\beta = (\cos \theta, -\sin \theta, 0)$, the equations (3.1) - (3.4) are reduced to

$$E = \frac{K}{8}(1 - \cos 4\psi) - H I_s \cos \phi$$
$$- \frac{3}{4}\sigma \left[\lambda_{100} + \frac{1}{2}(\lambda_{100}+\lambda_{111})\cos 2(\psi+\theta) + \frac{1}{2}(\lambda_{100}-\lambda_{111})\cos 2(\psi-\theta)\right] \tag{3.7}$$

For an iron crystal, $\lambda_{111} \simeq -\lambda_{100}$, so that now we assume $\lambda_{111} = -\lambda_{100}$ for convenience. Then eq. (3.7) can be reduced to the

following:

$$E = \frac{K}{8}(1 - \cos 4\psi) - HI_s \cos\phi - \frac{3}{4}\lambda_{100}\sigma[1 + \cos 2(\psi-\theta)] \tag{3.8}$$

It is convenient to express the parameters in non-dimensional form by dividing throughout by K. The non-dimensional energy η (=E/K) can be expressed as

$$\eta = \frac{1}{8}(1 - \cos 4\psi) - h\cos\phi - \frac{s}{4}[1 + \cos 2(\psi-\theta)] \tag{3.9}$$

and

$$h = \frac{H I_s}{K} \quad , \quad s = \frac{3\lambda_{100}\sigma}{K} \tag{3.10}$$

where h represents the non-dimensional field and s represents the non-dimensional stress. In eq. (3.9), the angles ψ, ϕ and θ are used; it is better to rewrite the equation by using only ϕ and θ as

$$\eta = \frac{1}{8}[1 - \cos 4(\phi-\theta)] - h\cos\phi - \frac{s}{4}[1 + \cos 2(\phi-2\theta)] \tag{3.11}$$

thus, η is a function of h, s, ϕ and θ. Treating h, s and θ as fixed, the stationary values of the function are given by

$$\frac{\partial\eta}{\partial\phi} = \frac{1}{2}\sin 4(\phi-\theta) + h\sin\phi + \frac{s}{2}\sin 2(\phi-2\theta) = 0 \tag{3.12}$$

and these correspond, respectively, to minima, points of inflection, or maxima for

$$\frac{\partial^2 \eta}{\partial \phi^2} = 2\cos 4(\phi-\theta) + h\cos\phi + s\cos 2(\phi-2\theta) \gtreqless 0 \qquad (3.13)$$

Figure 3.8 shows the relation between field and direction of magnetization for stationary values of the energy, which is calculated by solving eq. (3.12) for s = 0. Because of the symmetry of the crystal, the calculation was made in the range of $0° \leqq \theta \leqq 45°$. The arrows indicate the course of the change in ϕ as h is increased from -2.5.

In Fig. 3.8 (a) for $\theta = 0°$, as h is increased from -2.5 to a positive value, a discontinuous jump of ϕ occurs from $\phi = 180°$ to $\phi = 0°$ at h = 2. Physically, the discontinuous jump of ϕ corresponds to the discontinuous rotation of the magnetization vector. As h is decreased up to zero after the jump has occurred, the direction of the magnetization vector still remains at $\phi = 0°$. Further, if h is decreased from zero to a negative value, a discontinuous jump of ϕ occurs from $\phi = 0°$ to $\phi = 180°$ at h = -2. The critical point is represented by (ϕ_1, h_1) where the discontinuous jump occurs. This type of the behavior around the critical point is known as the unstable-symmetric bifurcation [9].

In Fig. 3.8 (b) for $\theta = 15°$, as h is increased from -2.5 to a positive value, a discontinuous jump occurs at the critical point (ϕ_1, h_1). In Fig. 3.8 (d) for $\theta = 30°$, as h is increased from -2.5 to a positive value, a discontinuous jump occurs at (ϕ_1, h_1), and further, another discontinuous jump occurs at (ϕ_2, h_2). In Fig. 3.8 (c) for $\theta = 22.5°$, the magnitudes of

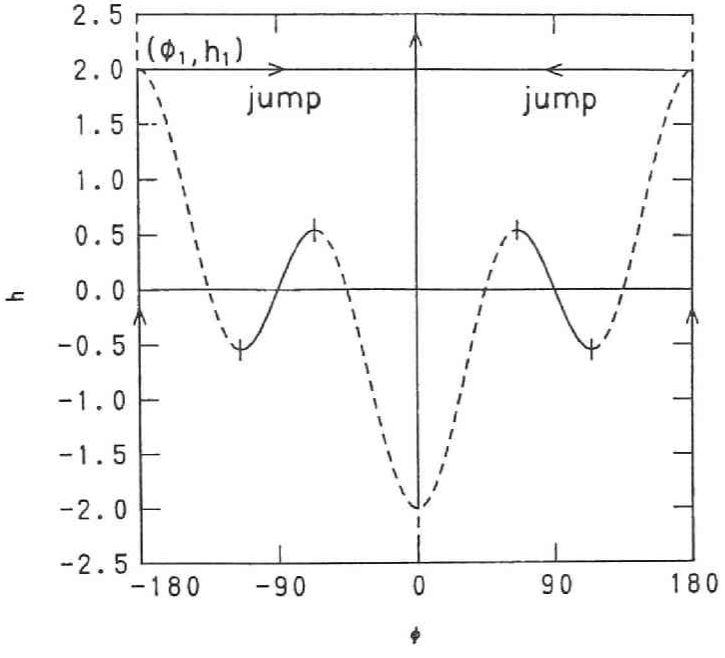

(a) $\theta = 0°$.

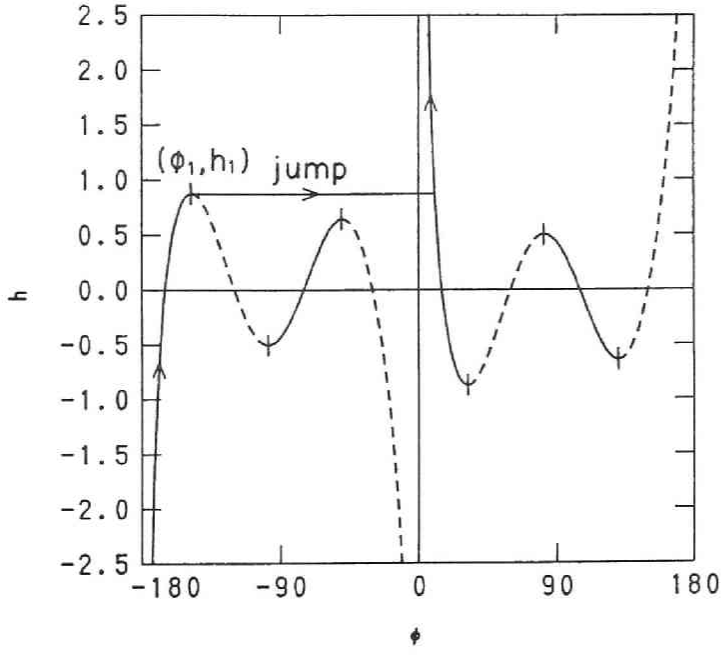

(b) $\theta = 15°$.

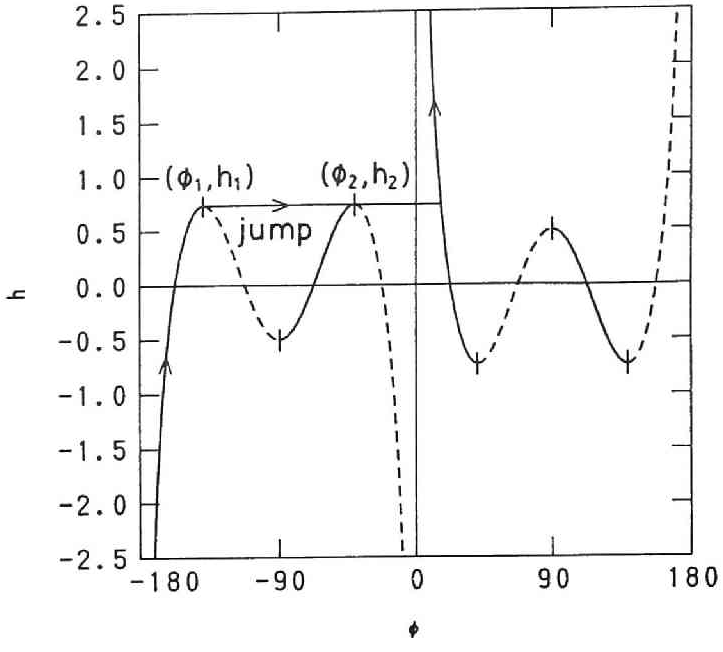
2.5
2.0
1.5
1.0
0.5
0.0
-0.5
-1.0
-1.5
-2.0
-2.5
h
(φ1,h1)
(φ2,h2)
jump
-180
-90
0
90
180
φ

(c) θ = 22.5°

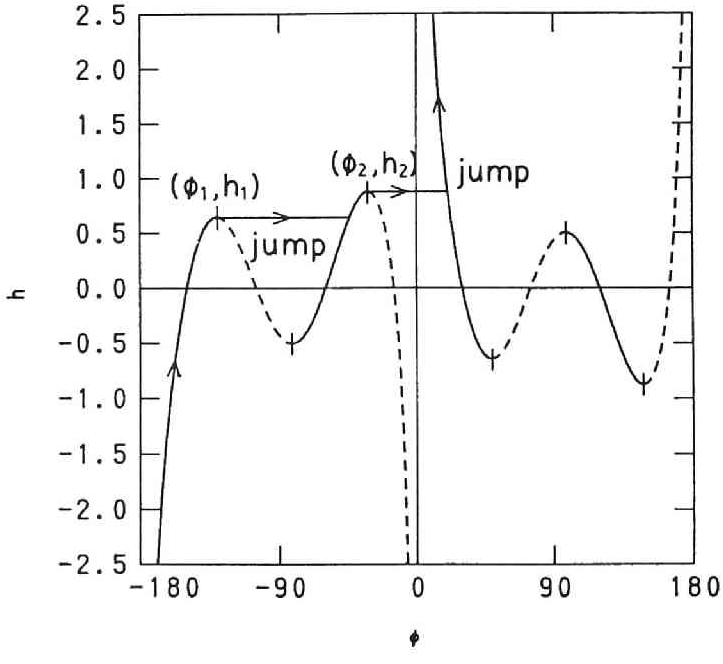
2.5
2.0
1.5
1.0
0.5
0.0
-0.5
-1.0
-1.5
-2.0
-2.5
h
(φ1,h1)
(φ2,h2)
jump
jump
-180
-90
0
90
180
φ

(d) θ = 30°

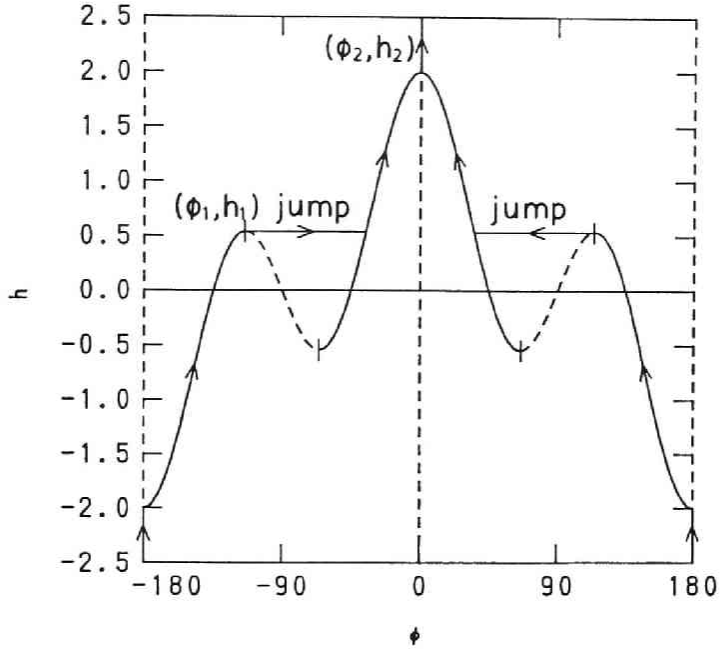

(e) $\theta = 45°$.

Fig. 3.8 Relationship between field and direction of magnetization for stationary values of the energy for stress $\sigma = 0$. h is the non-dimensional field ($= HI_s/K$) and ϕ is the angle between H and I_s. The full and broken parts of the curves correspond to the energy minima and maxima, respectively. The arrows indicate the course of the change in ϕ as h is increased from -2.5.

and h_2 are equal, thus the discontinuous jumps readily occur. Figure 3.8 (b) represents the feature for $0° < \theta < 22.5°$, and Fig. 3.8 (d) represents the feature for $22.5° < \theta < 45°$. This type of the behavior around the critical points is known as the asymmetric bifurcation [9].

In Fig. 3.8 (e) for $\theta = 45°$, as h is increased from -2.5 to a positive value, a discontinuous jump occurs at the critical point of (ϕ_1, h_1), but at the critical point (ϕ_2, h_2) such jump does not occur. The type of the behavior around (ϕ_1, h_1) is known as the asymmetric bifurcation, and the type of the behavior around (ϕ_2, h_2) is known as the stable-symmetric bifurcation [9].

3.4.2 Critical Values

Now we represent the critical values for ϕ_{crit} and h_{crit}, each of which consists of ϕ_1, ϕ_2 and h_1, h_2, respectively. These values are such that the first partial derivative of η with respect to ϕ being zero and the second one passes through zero from a positive to a negative value. The critical values thus can be obtained by solving the simultaneous equations (3.12) and (3.13) (with the equality sign). We now form the following equation for eliminating h_{crit}:

$$\left[\frac{1}{2}\sin 4(\phi_{crit} - \theta) + \frac{s}{2}\sin 2(\phi_{crit} - 2\theta)\right]\cos\phi_{crit} - \left[2\cos 4(\phi_{crit} - \theta) + s\cos 2(\phi_{crit} - 2\theta)\right]\sin\phi_{crit} = 0 \tag{3.14}$$

For given values of θ and s, the critical value ϕ_{crit} is

calculated by solving eq. (3.14) by successive approximations. Substituting ϕ_{crit} for ϕ in eqs. (3.12) and (3.13), we obtain the critical field h_{crit}.

The analytical results obtained are shown in Figs. 3.9 and 3.10. The value of s = 0.25 corresponds to the stress of σ = 190 MPa for iron. In the range of $0° \leqq \theta \leqq 22.5°$, the critical values of h_2 and ϕ_2 have no effect for the discontinuous jump because $h_2 < h_1$. In the range of $22.5° < \theta < 45°$, the magnetization vector rotates discontinuously at the critical point (ϕ_1, h_1), and further at (ϕ_2, h_2).

It can be seen in Fig. 3.10 that h_{crit} varies as the stress varies; i.e., h_{crit} increases with an increase of the stress in the range of $0.8 \lesssim h \lesssim 2.0$, and h_{crit} decreases with an increase of the stress in the range of $0.5 \lesssim h \lesssim 0.8$, where a positive stress indicates that it is tensile and a negative stress indicates that it is compressive. The specimen used in this experiment has all directions of θ (random orientation); therefore, the discontinuous rotation of magnetization vectors will occur as the tensile stress increases continuously in the range of $0.5 \lesssim h \lesssim 0.8$. On the other hand, the discontinuous rotation will not occur with a continuous increase of the tensile stress in the range of $0.8 \lesssim h \lesssim 2.0$.

The critical field h_{crit} has its maximum value at $\theta = 0°$ and $\theta = 45°$. The maximum value for $\theta = 0°$ or $\theta = 45°$ can be calculated by substituting $(\theta, \phi) = (0°, 0°)$ or $(45°, 180°)$ to eqs. (3.12) and (3.13), and has the same value as

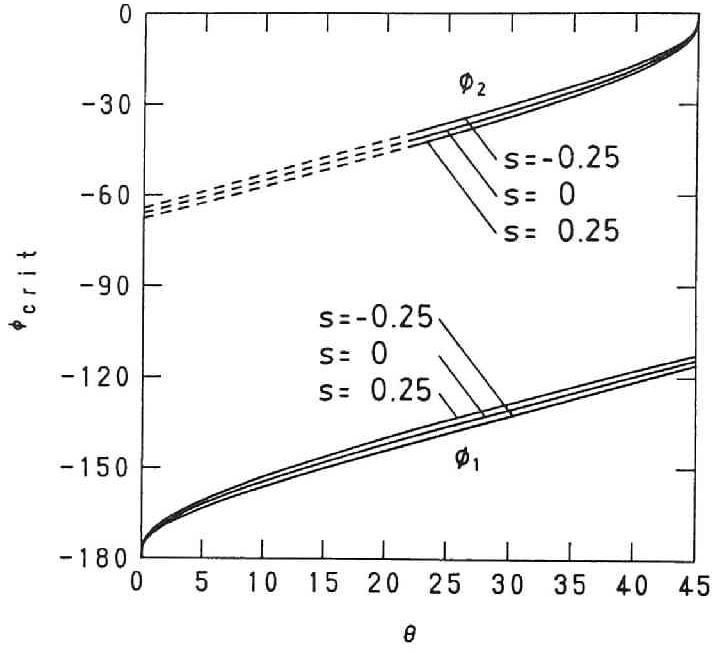

Fig. 3.9 Critical angles of magnetization ϕ_{crit} as a function of the direction of the crystal θ for the non-dimensional stresses of s = -0.25, 0, 0.25 ($s = 3\lambda_{100}\sigma/K$). Each of the full and the broken curves indicates the point of inflection of the energy. The discontinuous jump of ϕ occurs only on the full curves as h is increased from -2.5.

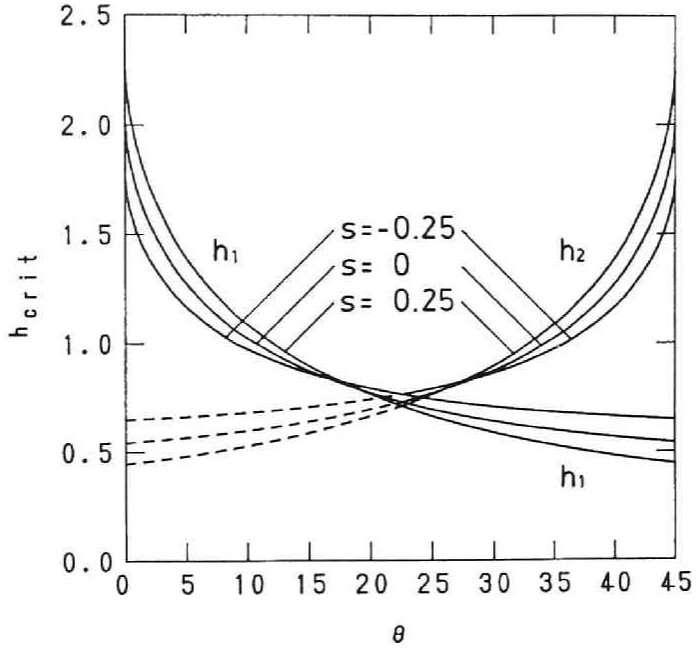

Fig. 3.10 Critical fields h_{crit} as a function of θ for s = -0.25, 0, 0.25. Each of the full and the broken curves indicates the point of inflection of the energy. The discontinuous jump of ϕ occurs only on the full curves as h is increased from -2.5.

$$(h_{crit})_{max} = 2 + s \tag{3.15}$$

or

$$H_{crit} = \frac{2K + 3\lambda_{100}\sigma}{I_s} \tag{3.16}$$

Note that the critical field H_{crit} corresponds to the maximum of the critical non-dimensional field, $(h_{crit})_{max}$. When $h \geq 2 + s$ ($H \geq H_{crit}$), the direction of a magnetization vector can be determined as a unique value as is clear from Fig. 3.8. This also indicates that if the applied field H is greater than H_{crit}, the state of magnetization is determined as unique and the hysteresis phenomenon can not be observed.

3.4.3 Comparison with the Experimental Results

In this subsection, the theoretical results are compared with the experimental results. μ_{min} in this experiment corresponds to the case where h has a high value greater than 2 ($h > 2$) in the initial state and is subsequently decreased up to the setting value of positive ($h > 0$). It is clear from Fig. 3.8 that magnetization can not change discontinuously in this case. Thus, the hysteresis due to applied stresses can not be observed in the theoretical prediction. In this experiment, the hysteresis was not observed when $H \geq 47.8$ kA/m, but it was seen when $H \leq 39.8$ kA/m. The theoretical critical field at $\sigma = 0$ is $H_{crit} = 44.5$ kA/m, which agrees well with the experimental critical field of $39.8 \text{ kA/m} < H < 47.8 \text{ kA/m}$. It can be said that the hysteresis did not occur when $H \geq H_{crit}$

because the magnetization state is unique.

However, the fact that the hysteresis occurred when $H < H_{crit}$ can not be explained by this theory. The origin of the hysteresis may be explained such as follows: the magnetization can have more than two stable equilibrium states when $H < H_{crit}$, so that it jumps over the energy block to the other equilibrium states for minimizing the total energy which contains the energy not treated here.

μ_{max} in this experiment corresponds to the case where h has a high value of negative less than -2 ($h < -2$) in the initial state and is then increased up to the setting value of positive ($h > 0$). In this case, the directions of I_s approach the direction of H, rotating continuously and discontinuously, as the applied field increases. It is predicted by the theory that the values of μ_{max} and μ_{min} are different when $H < H_{crit}$ and they are same when $H \geq H_{crit}$, which agrees well with the experimental results.

As already stated in Sec. 3.4.2, this theory predicts that the hysteresis of μ_{max} due to stress can occur only in the region of $0.5 \lesssim h \lesssim 0.8$, corresponding to 11.1 kA/m $\lesssim H \lesssim$ 17.8 kA/m, wherein h_{crit} decreases with an increase of tensile stress. In the experiment, the hysteresis occurred at H = 7.96 kA/m and 15.9 kA/m, and did not occur at H = 23.9 kA/m and more. The hysteresis at H = 7.96 kA/m can not be explained by this theory, but the fact that it occurred at H = 15.9 kA/m and did not occur at H = 23.9 kA/m and more agrees with this theory. However, it is more acceptable that the hysteresis at H = 7.96

kA/m and H = 15.9 kA/m occurred due to the domain wall movement, instead of the irreversible rotation of the magnetization vectors.

As described above, the absence of the hysteresis above a critical field has been explained by this theory, wherein it is assumed that the domain wall movement does not occur. However, since this assumption is invalid in low fields, this theory could not explain the hysteresis observed in low fields.

3.5 CONCLUSIONS

The hysteresis phenomenon in the relation between the reversible permeability and the stresses was examined experimentally and discussed theoretically. The results obtained are summarized as follows:

(1) The reversible permeabilities μ_{max} and μ_{min} were measured at the constant biasing field H under applied stresses. The values of μ_{max} and μ_{min} were different for $H \leq 39.8$ kA/m, but on the other hand, they were the same for $H \geq 47.8$ kA/m within the precision of the measurements. The nature was explained well by the theory proposed here.

(2) The hysteresis of μ_{min} was observed for $H \leq 39.8$ kA/m, and it was not observed for $H \geq 47.8$ kA/m. On the other hand, the hysteresis of μ_{max} was observed for $H \leq 15.9$ kA/m, and it was not observed for $H \geq 23.9$ kA/m. The mechanism of these hysteresis have not been clarified by the theory.

(3) The critical field, over which the state of the magnetization can be determined as unique and under which it

can not be determined as unique, was demonstrated as

$$H_{crit} = (2K + 3\lambda_{100}\sigma)/I_s.$$

For measuring stresses by using this method, the biasing field applied should be over the critical field.

APPENDIX FOR CHAPTER III

In this appendix section, the procedure to determine the reversible permeability μ_{rev} from the measured value of the inductance L is summarized. This procedure is mainly based on Ref. 3. It was programmed on a personal computer.

1. The values required are

   L (mH): inductance of A.C. coil with the specimen,

   L_0 (mH): inductance of A.C. coil in air,

   f (Hz): frequency for the measurement of the inductance,

   d (mm): diameter of the specimen,

   d_c (mm): diameter of A.C. coil, and

   ρ ($\mu\Omega$m): resistivity of the specimen.

2. Calculating c and y in the following formulas.

$$c = f\, d^2/(50600\, \rho) \tag{3.A1}$$

$$y = c\, [\, 1 + (L - L_0)\, d_c^{\,2}/(L_0\, d^2)\,] \tag{3.A2}$$

3. Solving the value f/f_g which satisfy the following equation by successive approximations, where f_g is called the limit frequency [10].

$$y = (f/f_g)\, P(f/f_g) \tag{3.A3}$$

and

$$P(f/f_g) = \frac{2}{f/f_g} \frac{M_1(f/f_g)}{M_0(f/f_g)} \sin(\theta_1-\theta_0-\pi/4) \qquad (3.A4)$$

where $M_0(z) = (ber^2 z + bei^2 z)^{1/2}$,

$M_1(z) = (ber_1^2 z + bei_1 z^2)^{1/2}$,

$\theta_0(z) = \tan^{-1}(bei\ z/ber\ z)$,

$\theta_1(z) = \tan^{-1}(bei_1 z/ber_1 z)$.

The Bessel functions ber, bei, ber_1 and bei_1 are tabulated by McLachlan [11]. The function $P(f/f_g)$ itself is also tabulated [10].

4. The reversible permeability μ_{rev} as a relative permeability (equal to 1 for air) can be calculated by the following formula.

$$\mu_{rev} = (f/f_g)\ c^{-1} \qquad (3.A5)$$

5. The skin thickness δ can also be obtained by the following formula.

$$\delta = \left(\frac{2}{f/f_g}\right)^{1/2} a \qquad (3.A6)$$

where a is the radius of the specimen (= d/2)

REFERENCES FOR CHAPTER III

[1] J. Iwayanagi and S. Abuku, Oyo Buturi, **34**, 492 (1965) (in Japanese).

[2] E. C. Stoner and E. P. Wohlfarth, Philos. Trans. R. Soc. London, **A240**, 599 (1948).

[3] S. Abuku and B. D. Cullity, Exp. Mech., **11**, 217 (1971).

[4] J. Iwayanagi, Rep. Ship Res. Inst., **12**, 67 (1975) (in Japanese).

[5] R. Becker and W. Döring, "Ferromagnetismus", Sec. 3 (1939) Springer, Berlin.

[6] R. M. Bozorth, "Ferromagnetism", p. 870 (1951) D. van Nostrand, Princeton.

[7] H. Gengnagel and U. Hofmann, Phys. Stat. Sol., **29**, 91 (1968).

[8] E. W. Lee, Rep. Prog. Phys., **18**, 185 (1955).

[9] A. B. Pippard, "Response and Stability: An Introduction to the Physical Theory", Chap. 5 (1985) Cambridge Univ. Press, Cambridge.

[10] R. C. McMaster, ed., "Nondestructive Testing Handbook", Chap. 36 (1959) Ronald Press, New York.

[11] N. W. McLachlan, "Bessel Functions for Engineers", second ed., Chap. 7 (1955) Clarendon Press, Oxford.

CHAPTER IV

EFFECT OF STRESS ON THE LAW OF APPROACH TO SATURATION MAGNETIZATION

4.1 INTRODUCTION

As described in the previous chapter, stress can be determined as a unique value when the magnetizing field is higher than the critical value. Under such high field, it is known that the law of approach to saturation magnetization is applicable. In this chapter, the effect of stress on the law is examined in order to apply the law for nondestructive stress measurement.

In high fields where the magnetization is approaching the saturation magnetization, the magnetization I can be expressed by power series of the inverse of external field H as

$$I = I_s - b/H^2 - c/H^3 - \ldots \qquad (4.1)$$

where I_s is the spontaneous magnetization and b, c are constants. The term of 1/H does not appear by the standard theoretical treatment although it has been observed in many experiments. The formula is referred to as the law of approach to saturation magnetization. The coefficients b, c have been calculated for

the materials that have the magnetocrystalline anisotropy [1-4]. The results for the polycrystalline materials are

$$b = 0.0762\ K^2/I_s \tag{4.2}$$

$$c = 0.0384\ K^3/I_s{}^2 \tag{4.3}$$

where K is the crystal anisotropy constant, the value of which is 47.2 kJ/m^3 for iron at room temperature [5]. The experiments carried out by Czerlinsky [6] and Polley [7] have shown that the values of K for iron and nickel determined from eq. (4.2) agree well with those directly determined from the properties of the single crystals, which validates the equation.

Following the calculation by Becker and Döring [3], the author calculated the coefficients b and c for a polycrystalline material subjected to the uniaxial stress whose direction was the same as that of the external field. In order to verify the theoretical formulas, measurements of reversible permeability in steel bars subjected to tension were carried out. The steel chords for prestressed concrete were also examined because of the importance of their engineering applications.

4.2 THEORY

In this section, the theoretical formula of law of approach to saturation magnetization including the effect of the stress is deduced. First, the calculation of the coefficients b, c by Becker and Döring is summarized [3]. Second, the calculation

of b, c including the effect of the stress is performed by the author based on the calculation by Becker and Döring.

4.2.1 Calculation by Becker and Döring

The direction cosines $\alpha = (\alpha_1, \alpha_2, \alpha_3)$, relative to the crystal axes (Fig. 4.1), of the spontaneous magnetization I_s are determined as the values giving the minimum of the potential

$$\psi(\alpha) = F(\alpha) - HI_s(\alpha_1\beta_1 + \alpha_2\beta_2 + \alpha_3\beta_3) \tag{4.4}$$

where $F(\alpha)$ is the dependence of the free energy for the direction α of the vector I_s, and H is the external field whose direction cosines are $\beta = (\beta_1, \beta_2, \beta_3)$. On the problem of minimizing $\psi(\alpha)$ under the condition $\Sigma\alpha_i^2 = 1$, adding the $(1/2)\ L\ (\alpha_1^2 + \alpha_2^2 + \alpha_3^2)$ to the potential $\psi(\alpha)$, where L is the factor of Lagrange, we obtain

$$G(\alpha) = \psi(\alpha) + (1/2)\ L\ (\alpha_1^2 + \alpha_2^2 + \alpha_3^2) \tag{4.5}$$

and minimize the potential $G(\alpha)$. The unknowns α_1, α_2, α_3 and L can be determined by solving the following simultaneous equations

$$\frac{\partial G}{\partial \alpha_i} = \frac{\partial F}{\partial \alpha_i} - H\ I_s\ \beta_i + L\ \alpha_i = 0 \quad (i = 1, 2, 3) \tag{4.6}$$

$$\Sigma\alpha_i^2 = 1 \tag{4.7}$$

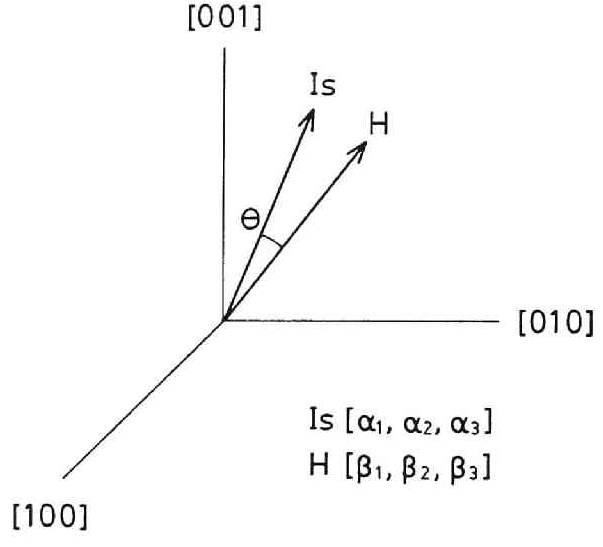

Fig. 4.1 The analytical model and the coordinate system of the crystal. I_s is the spontaneous magnetization and H is the external field.

Multiplying both sides of eq. (4.6) by $(HI_s)^{-1}$, then

$$\eta \frac{\partial F}{\partial \alpha_i} + \nu \alpha_i = \beta_i \qquad (i = 1, 2, 3) \tag{4.8}$$

where

$$\eta = \frac{1}{HI_s} \quad , \quad \nu = \frac{L}{HI_s} \tag{4.9}$$

As the external field H is greatly increased, η is decreased as $\eta \to 0$ and magnetization vector approaches the direction of external field, giving $\alpha_i \to \beta_i$, therefore $\nu \to 1$ from eq. (4.8). Therefore the unknowns can be expressed approximately by the power series of η as

$$\alpha_i = \beta_i + \eta A_i + \eta^2 B_i + \eta^3 C_i + \ldots \tag{4.10}$$

$$\nu = 1 + \eta \nu^{(1)} + \eta^2 \nu^{(2)} + \ldots \tag{4.11}$$

Substituting eq. (4.10) into eq. (4.7) and using $\Sigma \beta_i^2 = 1$, we obtain the next equations:

$$\Sigma \beta_i A_i = 0 \tag{4.12a}$$

$$\Sigma \beta_i B_i = -(1/2) \Sigma A_i^2 \tag{4.12b}$$

$$\Sigma \beta_i C_i = - \Sigma A_i B_i \tag{4.12c}$$

The resolved magnetization I in the direction of H is a project of I_s to the direction of H, and is then expressed by

using eqs. (4.10) and (4.12) as

$$I = I_s \cos\theta = I_s \sum \alpha_i \beta_i$$

$$= I_s [\ 1 - (1/2)\eta^2 \sum A_i^2 - \eta^3 \sum A_i B_i - \ldots\ ] \quad (4.13)$$

where θ is the angle between the vectors H and I_s as shown in Fig. 4.1. Note that the term 1/H does not appear in this equation for any expression of $F(\alpha)$.

Substituting the Taylor's series of $F(\alpha)$ in terms of β into eq. (4.8) and eliminating the factors of η and η^2, we finally obtain

$$\nu^{(1)} = - \sum F_i \beta_i \quad (4.14)$$

$$A_i = -F_i - \nu^{(1)} \beta_i \quad (4.15)$$

$$\sum A_i B_i = -\nu^{(1)} \sum A_i^2 - \sum A_i A_k F_{ik} \quad (4.16)$$

where

$$F_i = \left(\frac{\partial F}{\partial \alpha_i}\right)_{\alpha=\beta} , \quad F_{ik} = \left(\frac{\partial^2 F}{\partial \alpha_i \partial \alpha_k}\right)_{\alpha=\beta} \quad (4.17)$$

4.2.2 Calculation of the coefficients b and c including the effect of stress

When the uniaxial stress σ is applied to a single cubic crystal in the direction of the external field H, $F(\alpha)$ is expressed as follows [8]:

$$F(\alpha) = K (\alpha_1^2\alpha_2^2 + \alpha_2^2\alpha_3^2 + \alpha_3^2\alpha_1^2) - (3/2)\sigma [\lambda_{100}(\alpha_1^2\beta_1^2 + \alpha_2^2\beta_2^2 + \alpha_3^2\beta_3^2) + 2\lambda_{111} (\alpha_1\alpha_2\beta_1\beta_2 + \alpha_2\alpha_3\beta_2\beta_3 + \alpha_3\alpha_1\beta_3\beta_1)] \quad (4.18)$$

where K is the crystal anisotropy constant and λ_{100}, λ_{111} are the magnetostriction constants. Equation (4.18) can be rewritten as

$$F(\alpha) = (1/2)K [1 - \alpha_i^4] - (3/2)(\lambda_{100} - \lambda_{111})\sigma \Sigma\alpha_i^2\beta_i^2 - (3/2) \lambda_{111}\sigma [\Sigma \alpha_i \beta_i]^2 \quad (4.19)$$

Calculating eq. (4.17) for F(α) of eq. (4.19), we obtain

$$F_i = -2K'\beta_i^3 - 3\lambda_{111}\sigma \beta_i \quad (4.20a)$$

$$F_{ik} = -(6K + 3\lambda_{100}\sigma)\beta_i^2 \quad \text{(for } i=k\text{)} \quad (4.20b)$$

$$F_{ik} = -3\lambda_{111}\sigma \beta_i\beta_k \quad \text{(for } i\neq k\text{)} \quad (4.20c)$$

where

$$K' = K + (3/2)(\lambda_{100} - \lambda_{111})\sigma \quad (4.21)$$

Calculating eqs. (4.14) and (4.15) for eq. (4.20), we obtain

$$\Sigma A_i^2 = 4K'^2 (S_6 - S_4^2) \quad (4.22)$$

where $S_4 = \Sigma\beta_i^4$ and $S_6 = \Sigma\beta_i^6$. By using the next identical relation

$$\Sigma\,(\,\beta_i^2 - S_4\,)(\,\beta_k^2 - S_4\,)\beta_i^2\beta_k^2 = 0 \qquad (4.23)$$

equation (4.16) can be calculated as

$$\begin{aligned}\Sigma\, A_iB_i = 8K'^3[\, & K(\,3S_8 - 7S_4S_6 + 4S_4^3\,) \\ & + (3/2)(\,\lambda_{100} - \lambda_{111}\,)\sigma\,(\,S_8 - 3S_4S_6 + 2S_4^3\,) \\ & - (3/2)\,\lambda_{111}\sigma\,(\,S_6 - S_4^2\,)\,]\end{aligned} \qquad (4.24)$$

where $S_8 = \Sigma\beta_i^8$.

Equations (4.22) and (4.24) give the coefficients b and c for a single crystal, respectively. Replacing S_4, S_6, etc. by their mean values, corresponding to a random orientation of crystals, we finally obtain for a polycrystal as follows:

$$b = 0.0762/I_s\,[\,K + 1.5(\,\lambda_{100} - \lambda_{111})\sigma\,]^2 \qquad (4.25)$$

$$\begin{aligned}c = {} & 0.0384/I_s^2[\,K + 1.5(\,\lambda_{100} - \lambda_{111})\sigma\,]^2 \\ & \times [\,K - 4.67(\,\lambda_{100} - \lambda_{111})\sigma - 11.9\,\lambda_{111}\sigma\,]\end{aligned} \qquad (4.26)$$

These equations agree with eqs. (4.2) and (4.3), respectively, when stress σ is zero.

In general, we can measure the reversible permeability more precisely than the magnetization itself. Thus, the theoretical formula will be verified for the following formula:

$$\mu_{rev} = \frac{\partial B}{\partial H}\frac{1}{\mu_0} = 1 + \frac{\partial I}{\partial H}\frac{1}{\mu_0}$$
$$= 1 + (2b/H^3 + 3c/H^4 + \ldots)/\mu_0 \qquad (4.27)$$

where μ_{rev} is the reversible permeability in the dimensionless form, B is the flux density, I is the resolved magnetization, H is the biasing field, and μ_0 is the permeability of free space ($4\pi x10^{-7}$ H/m).

4.3 EXPERIMENTAL PROCEDURE

The materials used were cold-drawn rods of carbon steel of SS41 and S45C in JIS code, and steel chords for prestressed concrete, which are referred to here as PC(A) and PC(C). The chemical compositions are shown in Table 4.1. The specimens of SS41 and S45C have a length of 900 mm and a diameter of 10 mm, and those of PC(A) and PC(C) have a length of 900 mm and a diameter of 9.1 mm. The specimens of SS41 and S45C were annealed at 650°C for 90 minutes in vacuum and cooled naturally in the furnace. The same types of specimens without annealing (as drawn) were also used. The specimens of PC(A) and PC(C) were used only as drawn. The mechanical properties and the resistivity of the specimens are shown in Table 4.2. The values of the resistivity were measured by using a double bridge (Yokogawa 2752).

TABLE 4.1

CHEMICAL COMPOSITIONS OF THE MATERIALS IN WEIGHT %

Material	C	Si	Mn	P	S
SS41	0.18	0.27	1.08	0.013	0.006
S45C	0.44	0.14	0.77	0.017	0.018
PC(A)	0.30	1.65	0.52	0.012	0.005
PC(C)	0.30	0.26	0.83	0.010	0.006

TABLE 4.2

MECHANICAL PROPERTIES AND RESISTIVITY OF THE SPECIMENS

Specimen	Tensile strength	Yield strength	Rockwell hardness	Resistivity
	MPa	MPa		μΩm
SS41(annealed)	450	278	70(B)	0.190
SS41(as drawn)	621	---	93(B)	0.196
S45C(annealed)	633	496	92(B)	0.188
S45C(as drawn)	796	---	101(B)	0.202
PC(A)	1496	---	41(C)	0.387
PC(C)	1152	---	32(C)	0.210

The measuring setup used is the same as used in Chapter III, and is shown in Fig. 3.1. The inductances of the specimens were measured at the biasing fields of H = 55.2, 58.6, 63.2, 69.5, 79.6, 100.3 kA/m, the values of which are arranged at the regular intervals in the dimension of $1/H^3$, under the constant applied tension within the elastic limit. The frequency for the measurement of the inductance is 1020 Hz and the amplitude of the alternative fields is around 40 A/m. The setting speed of biasing fields did not affect the inductance in this experiment because the biasing fields applied were high

enough, thus the setting time was chosen as 2.6 μs/(A/m).

4.4 EXPERIMENTAL RESULTS

Figure 4.2 shows the relationship between the reversible permeability μ_{rev} and the biasing field H in the dimension of $1/H^3$ for various applied stresses. It can be seen that μ_{rev} varies linearly with $1/H^3$ and the slopes of the curves in the μ_{rev} - $1/H^3$ relation increase monotonously with an increase of the applied stresses. The intercepts of the curves are close to the value of 1.0 and are almost constant for the applied stresses.

We can express the experimental relations by the following formula:

$$\mu_{rev} = 1 + \chi_0 + M/H^3 \qquad (4.28)$$

where χ_0 represents the deflection of the intercept from 1.0 and M represents the slope of the curve in the μ_{rev} - $1/H^3$ relation. In this formula, χ_0 indicates the same quantity as the high field susceptibility [9]. Some of the values in this experiment are considerably higher than the value of 3.34×10^{-3} determined from the precise measurement [10]. However, we require only the values of M, which are varied by the applied stresses, so the lack of the precision in determining χ_0 does not affect the results described below.

In Fig. 4.2 (a) for annealed SS41 specimen, nonlinearity of the curve enlarges as the applied stress increases.

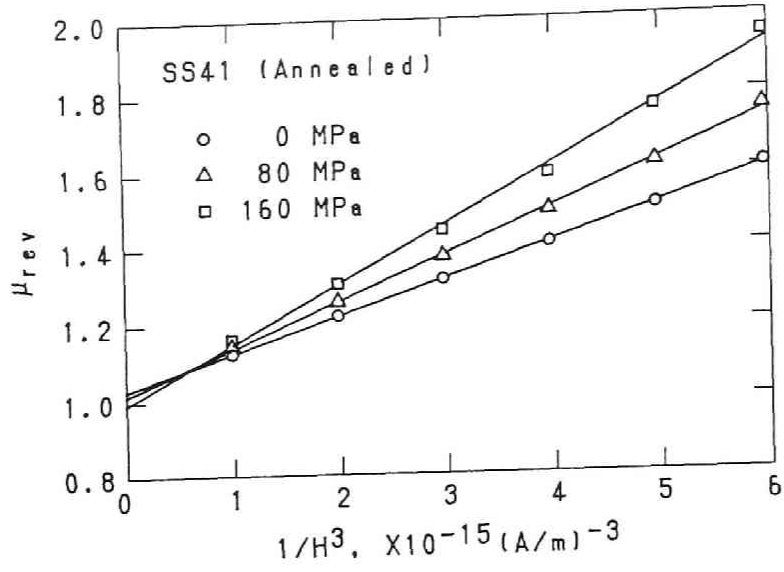

(a) SS41 (Annealed)

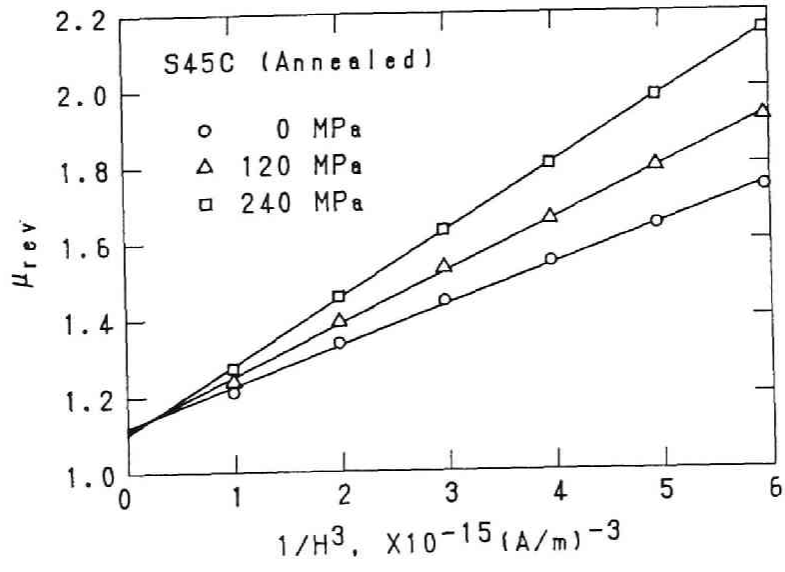

(b) S45C (Annealed)

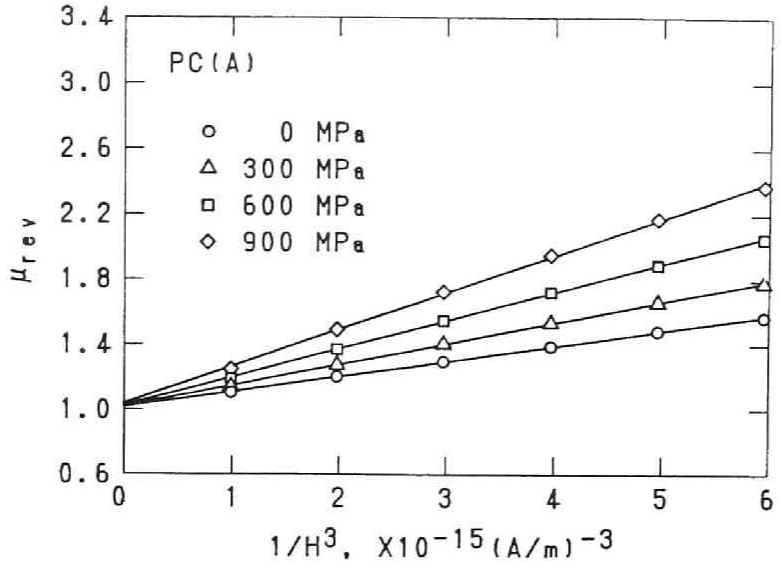

(c) PC(A)

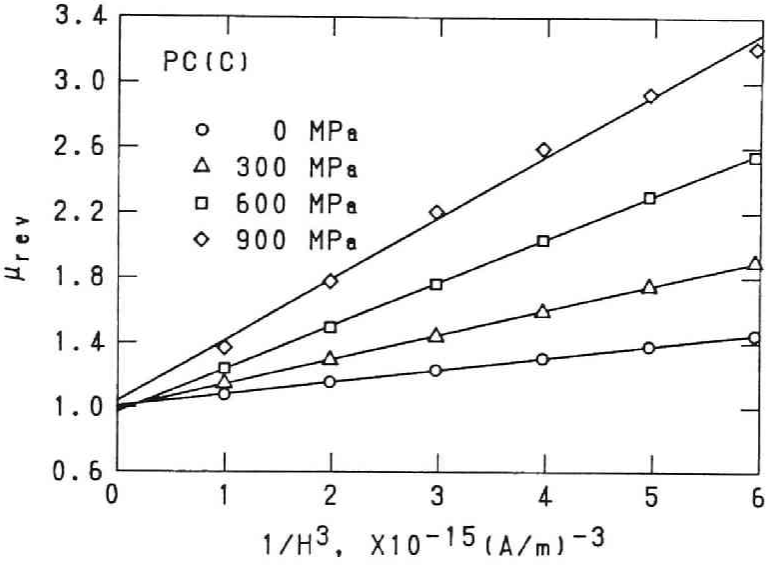

(d) PC(C)

Fig. 4.2 Relationship between the reversible permeability μ_{rev} and the biasing field H in the dimension of $1/H^3$ for various applied stresses.

The nonlinearity suggests that $1/H^4$ term also exists in eq. (4.28) and the term increases as the stress increases. In Fig. 4.2 (b) for annealed S45C specimen and in Fig. 4.2 (c) for PC(A) specimen, all of the curves seem almost linear and nonlinearity is not so apparent. This means that eq. (4.28) is followed well by these experimental results. In Fig. 4.2 (d) for PC(C) specimen, the curves for σ = 0, 300, 600 MPa are almost linear, but the curve for σ = 900 MPa indicates some nonlinearity. The nonlinearity is not the same as that for annealed SS41 specimen; the signature of curvature is opposite to that for annealed SS41 specimen. For the specimens of SS41 (as drawn) and S45C (as drawn), nonlinearity in μ_{rev} - $1/H^3$ relation is not so apparent and they can be expressed well with eq. (4.28).

Figure 4.3 shows the variation of square root of the slope M with applied stress σ. With an increase in stress, $\sqrt{M}$ increases linearly up to the maximum stress applied. In addition, hysteresis due to stress was not observed. Therefore, $\sqrt{M}$ can be expressed as a linear equation with respect to σ as follows:

$$\sqrt{M} = A + B\,\sigma \tag{4.29}$$

where A and B are constants and are defined here as the initial value and the stress sensitivity, respectively.

Nonlinearity of the curves in Figs. 4.3 (a) - (c) are not so apparent, but slightly positive nonlinearity can be seen

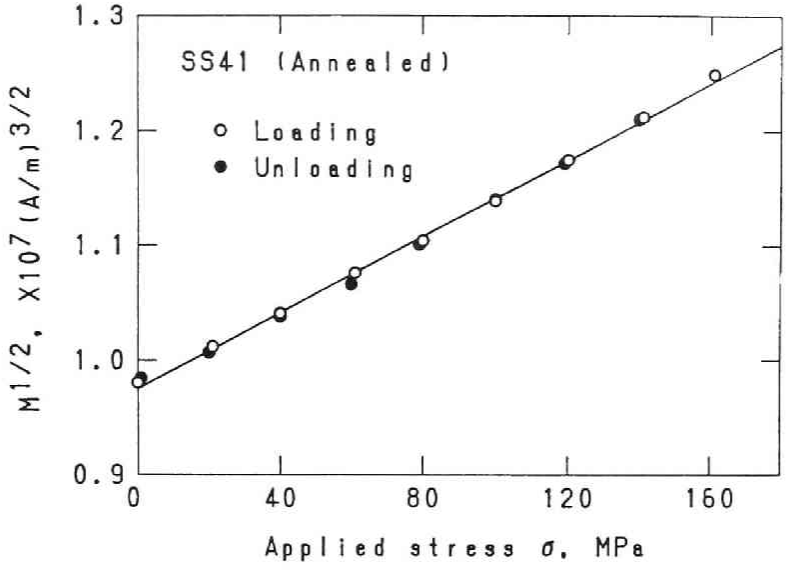

(a) SS41 (Annealed)

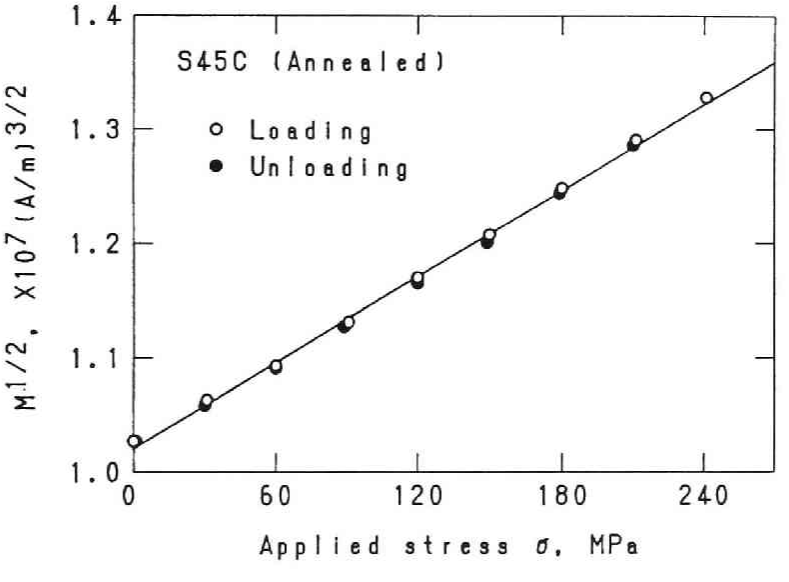

(b) S45C (Annealed)

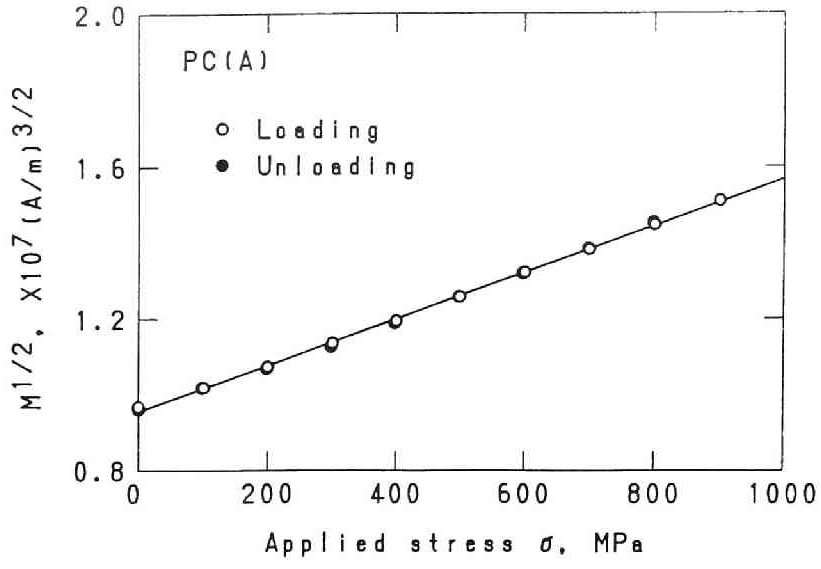

(c) PC(A)

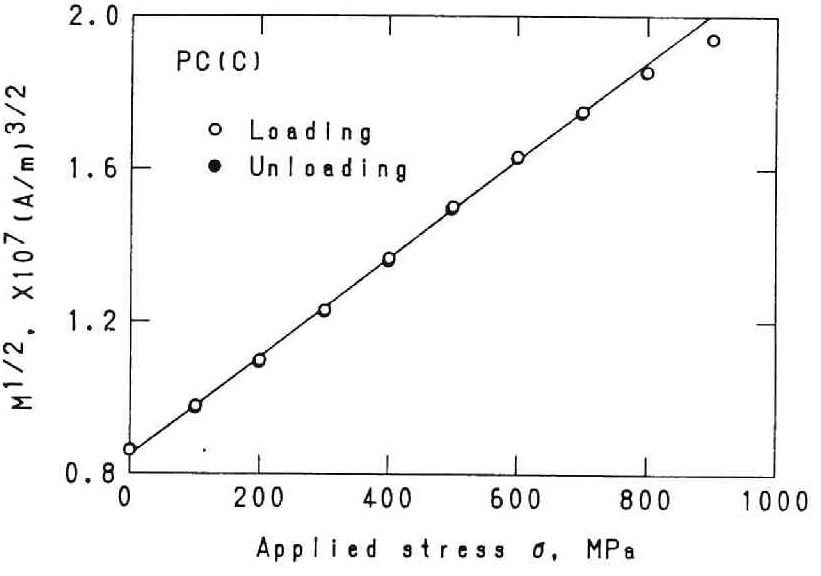

(d) PC(C)

Fig. 4.3 Variation of square root of the slope in μ_{rev} - $1/H^3$ relation, $\sqrt{M}$, with applied stress σ.

in Fig. 4.3 (a) for annealed SS41 specimen. In Fig. 4.3 (d) for PC(C) specimen, the curve is almost linear up to 700 MPa, but the data over σ = 800 MPa do not fit the linear relation. A phenomenon like this could be observed only in this case. For the specimens of SS41 (as drawn) and S45C (as drawn), the nonlinearity in $\sqrt{M}$ - σ relation was not so apparent and they could be expressed well with eq. (4.29). The values of A and B obtained are shown in Table 4.3.

TABLE 4.3

EXPERIMENTAL RESULTS AND THE STANDARD VALUES

Specimen	A	B	I_s	K	$\lambda_{100} - \lambda_{111}$
	$(A/m)^{3/2}$	$(A/m)^{3/2}/GPa$	T	kJ/m^3	
SS41(annealed)	9.73×10^{6}	16.70×10^{6}	2.02	39.7	45.5×10^{-6}
SS41(as drawn)	9.82	14.18	2.03	40.2	38.7
S45C(annealed)	10.19	12.59	1.97	41.1	33.9
S45C(as drawn)	10.55	10.53	1.98	42.7	28.4
PC(A)	9.53	6.16	1.95	38.2	16.5
PC(C)	8.48	12.87	2.02	34.6	35.0
Standard value	11.28	15.02	2.12*	47.2**	41.9***

* Bozorth [11], ** Gengnagel and Hofmann [5], *** Lee [12].

From the theoretical formulas of eqs. (4.25) and (4.27), the values of A and B can be expressed by the magnetic constants as follows:

$$A = 348\ K\ /\ \sqrt{I_s} \tag{4.30}$$

$$B = 522 \left(\lambda_{100} - \lambda_{111} \right) / \sqrt{I_s} \qquad (4.31)$$

The magnetic constants K and $(\lambda_{100} - \lambda_{111})$ were calculated from the experimental values of A, B and I_s by using eqs. (4.30) and (4.31). The values of the spontaneous magnetization I_s were determined experimentally by using a search coil and a flux meter (Yokogawa 3254). These values are shown in Table 4.3 with their standard values. It can be seen that all of the experimental values agree fairly well with their standard values. Therefore, the theoretical formula of eq. (4.25) can be said to be verified by this experiment.

4.5 DISCUSSION

4.5.1 Allowable Range of Biasing Field

In this subsection, the nature of the nonlinearity observed in PC(C) specimen is discussed below. From the theory presented in Chapter III, the critical field H_{crit} under applied stress is calculated as,

$$H_{crit} = (2K + 3 \lambda_{100} \sigma) / I_s . \qquad (4.32)$$

The critical field gives the critical value that the state of the magnetization is determined as unique; in other words, when $H \geq H_{crit}$ the magnetization has only one value, but when $H < H_{crit}$ the magnetization can have different values.

Table 4.4 shows the maximum stress applied in the experiment, the critical field in stress-free state, and the

critical field wherein the maximum stress is applied. The critical field increases linearly with an increase of stress from $2K/I_s$ to $(2K+3\lambda_{100}\ \sigma_{max})/I_s$.

TABLE 4.4

CRITICAL FIELDS

Specimen	σ_{max}	H_{crit}*	
		at $\sigma = 0$	at $\sigma = \sigma_{max}$
	MPa	kA/m	
SS41(annealed)	160	39.6	44.2
SS41(as drawn)	160	39.3	44.7
S45C(annealed)	240	43.0	48.2
S45C(as drawn)	240	41.7	47.9
PC(A)	900	39.2	50.6
PC(C)	900	34.2	57.6

* λ_{100} is determined from $(\lambda_{100} - \lambda_{111})/2$ by assuming $\lambda_{100} = -\lambda_{111}$.

It can be seen that the maximum critical field is for PC(C) specimen and it is greater than the biasing field of H = 55.1 kA/m applied in this experiment. The critical fields for the other specimens are less than the biasing field of H = 55.1 kA/m. This suggests that the nature of the nonlinearity in $\sqrt{M}$ - σ relation for PC(C) specimen occurred because the critical field became larger than the biasing field, H = 55.1 kA/m, applied in the experiment as stress increased. In fact, the nonlinearity occurred only when the applied stress was 800 MPa and 900 MPa, corresponding to H_{crit} = 55.0 kA/m and H_{crit} = 57.6 kA/m, respectively. In addition, after the elimination of the data at H = 55.1 kA/m for σ = 800 MPa and

σ = 900 MPa, the experimental relation became linear in both μ_{rev} - $1/H^3$ relation and $\sqrt{M}$ - σ relation. Therefore, it can be stated that the biasing field should be greater than the critical field defined by eq. (4.32).

4.5.2 Effect of $1/H^4$ Term

In the empirical formula of eq. (4.28), the term of $1/H^4$, which appears in the theoretical formula as shown in eq. (4.26), is omitted. In the following, the effect of the $1/H^4$ term is examined on the basis of the theoretical formula.

Equations (4.25) - (4.27) can be expressed by considering up to $1/H^4$ term and assuming $\lambda_{100} = -\lambda_{111}$ as follows:

$$\mu_{rev} = 1 + (2b'/h^3 + 3c'/h^4) I_s^2/(\mu_0 K) \qquad (4.33)$$

$$b' = 0.0762 (1 + s)^2 \qquad (4.34)$$

$$c' = 0.0384 (1 + s)^2 (1 + 0.85s) \qquad (4.35)$$

where

$$h = HI_s/K \qquad (4.36)$$

$$s = 1.5 (\lambda_{100} - \lambda_{111})\sigma /K \qquad (4.37)$$

In the formulas, h and s represent dimensionless parameters of the magnetic field H and the stress σ, respectively, where h = 1 corresponds to H = 22.3 kA/m and s = 1 corresponds to

σ = 751 MPa for iron.

In Fig. 4.4, the theoretical curves of χ_{rev} - h relation ($\chi_{rev} = \mu_{rev} - 1$) are plotted both for the formula up to $1/h^3$ term and that up to $1/h^4$ term. It is clear that the $1/h^4$ term causes slight nonlinearity in the χ_{rev} - $1/h^3$ relation. The nonlinearity is the same as in annealed SS41 specimen as shown in Fig. 4.2 (a). Equation (4.35) also indicates that the nonlinearity increases as the stress increases because of the term (1 + 0.85s). This agrees with the experimental results obtained for annealed SS41 specimen.

Next, the effect of the $1/H^4$ term to the $\sqrt{M}$ - σ relation is considered. Equations (4.33) - (4.35) can be expressed as follows:

$$\mu_{rev} = 1 + m/h^3 \, I_s^2/(\mu_0 K) \tag{4.38}$$

$$\sqrt{m} = 0.390(1 + s) \sqrt{1 + 0.756(1 + 0.85s)/h} \tag{4.39}$$

where m represents a dimensionless parameter of M. If h has an infinite value, $\sqrt{m}$ is a linear function of s. However, h has values ranging from 2.48 to 4.50 in this experiment, so $\sqrt{m}$ becomes a nonlinear function of s. The relation between $\sqrt{m}$ and s is plotted in Fig. 4.5 for h = ∞ and h = 3. Slight nonlinearity can be seen in the curve for h = 3. The nonlinearity is the same as that observed in the experiment for annealed SS41 specimen.

From the agreement between the theory up to $1/H^4$ term and

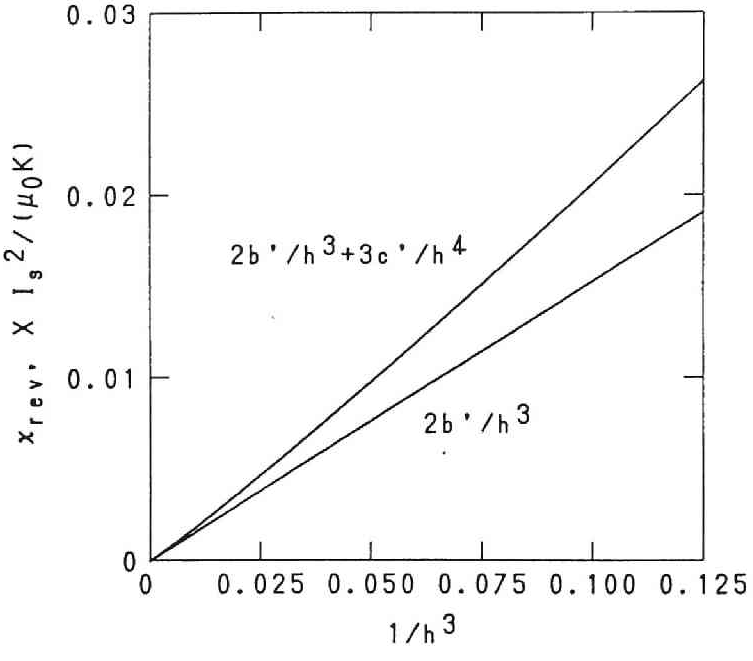

Fig. 4.4 Theoretical relationship between the reversible permeability and the non-dimensional field h ($=HI_s/K$) for each of the formulas up to $1/h^3$ term and $1/h^4$ term.

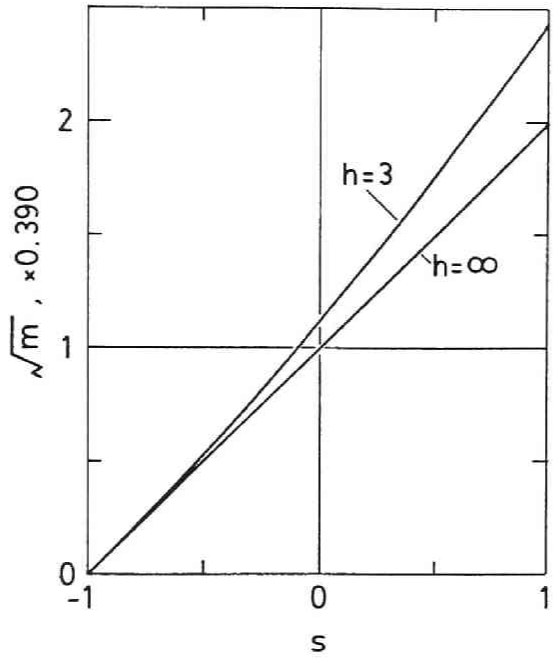

Fig. 4.5 Theoretical relationship between $\sqrt{m}$ and s for the values of h = 3 and ∞. The symbols m, s and h represent the dimensionless parameters of M, σ and H, respectively. m is determined as $\mu_{rev} = 1 + m/h^3$. $s = 3\lambda_{100}\sigma/K$.

the experiment for annealed SS41 specimen, it can be said that the nonlinearity in this specimen is caused by the $1/H^4$ term that the theory predicts as eq. (4.16). However, the nonlinearity was not apparent for the other specimens. The reason is not clear; the term of $1/H^2$, which is said to be caused by the stress field around dislocations or the nonmagnetic inclusions [13], may cancel the effect of the $1/H^4$ term.

4.5.3 Influence of Composition and Treatment

In Table 4.3, the values of the spontaneous magnetization are almost constant, but other coefficients vary with the specimens. If I_s has a constant value, the initial value A and the stress sensitivity B are proportional to the anisotropy constant K and the difference of the magnetostriction constants $(\lambda_{100} - \lambda_{111})$, respectively. Thus the discussion about the coefficients K and $(\lambda_{100} - \lambda_{111})$ are interchangeable for that about A and B, respectively, and vice versa.

The initial value A slightly decreases by annealing as shown in Table 4.3. The differences between A for as-drawn specimen and that for annealed specimen seem small; in fact, they are only 0.9 % for SS41 and 3.5 % for S45C. The corresponding errors in the stress determination are, however, 6 MPa for SS41 and 34 MPa for S45C. These errors are not negligible, and so precise calibration is required in order to predict the accurate initial value.

Figure 4.6 shows the variation of $(\lambda_{100} - \lambda_{111})$ with carbon content of the specimen. The value of $(\lambda_{100} - \lambda_{111})$ decreases

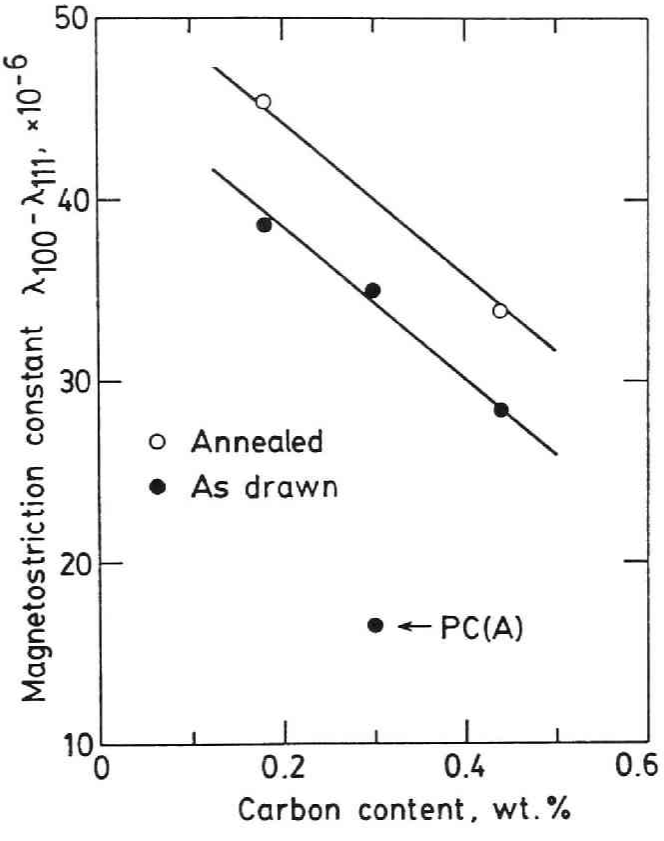

Fig. 4.6 Variation of the difference of the magnetostriction constants $\lambda_{100} - \lambda_{111}$ with carbon content of the specimens.

with an increase in carbon content, and increases by annealing except for PC(A) specimen. The apparent decrease of (λ_{100} - λ_{111}) of PC(A) specimen may be caused by a large silicon content, resulting in a large value of resistivity, as shown in Table 4.1. In fact, Carr and Smoluchowski [14] indicated that the value of (λ_{100} - λ_{111}) for iron-silicon alloys decreased as silicon increased by measuring the single crystals. Their data indicate that the decrease should be 3.7×10^{-6} when the silicon content varies from 0.26% to 1.65%. This value is considerably less than the obtained experimental value of 18.5×10^{-6}, so other factors such as the difference in treatment may cause the effect.

Carbon dependence of the stress sensitivity was measured by Iwayanagi and Abuku [15,16] for the magnetization change under constant biasing field up to 24 kA/m. Their results for annealed carbon steel at 14.3 kA/m indicate that the reduction of the stress sensitivity is -20% when the carbon content varies from 0.18% to 0.44% [16]. The value obtained in this experiment was -25%, which agrees well with -20%. Iwayanagi [17] suggested that the decrease of the stress sensitivity with carbon content might be due to the magnetostatic energy induced in the pearlite crystals. This suggestion, however, does not explain the fact that the data for PC(C) specimen, which has the martensite structure instead of pearlite, also fit the same line as that obtained for SS41 and S45C, which have the ferrite-pearlite structure.

The exact nature of the increase of the stress sensitivity

by annealing is not clear, but this is probably due to the release of the dislocations or reduction of the residual stresses. It is known that the dislocations and the nonmagnetic inclusions have influence on the 1/H term in eq. (4.1) [18]. In this experiment, we could not find out the apparent relationship between the 1/H term and the magnetic constants; this should be examined in the further research.

4.6 CONCLUSIONS

The effect of stress on the law of approach to saturation magnetization was studied theoretically and experimentally. The results obtained are summarized as follows:

(1) The coefficients of the formula referred to as the law of approach to saturation magnetization which include the effect of stress were deduced theoretically. They are shown in eqs. (4.22) and (4.24) for a single crystal and in eqs. (4.25) and (4.26) for a polycrystal.

(2) The values of reversible permeability μ_{rev} under applied tension were measured for mild-steel bars and steel chords used for prestressed concrete. The results showed that μ_{rev} increased linearly with an increase of $1/H^3$, and $\sqrt{M}$ changed linearly with applied stress σ, where M means the slope in μ_{rev}-$1/H^3$ relation. The values of the anisotropy constant K and the difference of the magnetostriction constants ($\lambda_{100} - \lambda_{111}$) were calculated on the basis of the theoretical formula of eq. (4.25). The calculated experimental values agreed fairly well with the standard values. Therefore, the theoretical formula of eq.

(4.25) was verified by this experiment.

(3) Allowable range of biasing field was discussed. Experimental results agreed with the theory presented in Chapter. III, namely, critical field of $H_{crit} = (2K+3\lambda_{100}\sigma)/I_s$. It was shown that the biasing field should be greater than the critical field.

(4) The effect of $1/H^4$ term was discussed theoretically. The term causes the nonlinearity in both μ_{rev}-$1/H^3$ relation and $\sqrt{M}$-σ relation. The nonlinearity was observed in the experimental results for annealed SS41 specimen.

(5) Influence on composition and treatment of specimens was discussed. Experimental results showed that the stress sensitivity decreased with an increase of carbon and silicon content, and increased by annealing.

APPENDIX FOR CHAPTER IV

In this appendix section, the measurement error of stress by using the magnetic method described in this chapter is discussed. Stress of the measuring object can be determined on the basis of the following formula as

$$\sigma_{meas} = (\sqrt{M} - A)/B \qquad (4.A1)$$

where σ_{meas} is the measured stress, $\sqrt{M}$ is the magnetic output, and A and B are the coefficients which should be determined in advance. We now estimate the measurement error for the three cases: (Case I) A is unknown and B is known, (Case II) A is known and B is unknown, and (Case III) both A and B are known.

Case I: A is unknown and B is known

Because the measurement error of stress is caused mainly by the estimation error of the initial value A in this case, we now estimate the error only by the estimation error of A. Then,

$$\sigma_{meas} = (\sqrt{M} - A')/B \qquad (4.A2)$$

$$\sigma_{true} = (\sqrt{M} - A)/B \qquad (4.A3)$$

$$\begin{aligned} \Delta\sigma &= \sigma_{meas} - \sigma_{true} \\ &= (A - A')/B \end{aligned} \qquad (4.A4)$$

where σ_{meas} is the measured stress, σ_{true} is the true stress, $\Delta\sigma$ is the measurement error of the stress, A' is the initial value predicted, and A and B are the true coefficients.

Case II: A is known and B is unknown

In this case, the measurement error is caused mainly by the estimation error of the stress sensitivity B, so that we now estimate the error only by B. Then,

$$\sigma_{meas} = (\sqrt{M} - A)/B' = \sigma_{true} (B/B') \quad (4.A5)$$

$$\Delta\sigma = \sigma_{meas} - \sigma_{true} = \sigma_{true} (B - B')/B' \quad (4.A6)$$

where B' is the stress sensitivity predicted, and the other symbols are the same as those in Case I.

Case III: both A and B are known

In this case, we can not predict the measurement error theoretically. Thus, we estimate it from the experimental data as

$$\Delta\sigma = \sigma_{meas} - \sigma_{appl} \quad (4.A7)$$

where σ_{meas} is the measured stress by using eq. (4.A1) in which the coefficients A and B are determined by the measured specimens

themselves, and σ_{appl} is the applied stress.

The measurement errors in this experiment are shown in Table 4.A1 for the three cases. For Cases I and II, the standard values of A and B shown in Table 4.3 are used as the coefficients A' and B', respectively. The experimental values shown in Table 4.3 are used as the true coefficients A and B. For Case III, the maximum values of $\Delta\sigma$ are shown in Table 4.A1.

TABLE 4.A1

MEASUREMENT ERROR OF STRESS

Specimen	Case		
	I	II	III
	MPa	%	MPa
SS41(annealed)	-93	11.2	4
SS41(as drawn)	-103	-5.6	4
S45C(annealed)	-87	-16.2	6
S45C(as drawn)	-69	-29.9	9
PC(A)	-284	-59.0	24
PC(C)	-218	-14.3	11*

* Maximum error in the region of $0 \leq \sigma \leq 700$ MPa.

It can be seen in Table 4.A1 that the errors in the Case I are considerably large and are not acceptable for stress measurement. Thus, the theoretical value of the initial value A can not be used; its calibration has to be performed. In Case II, the error is considerably large for the specimen of PC(A) and large for S45C(as drawn), but it is within ±20% for the other specimens. The stress sensitivity B is decreased linearly with an increase of carbon content as shown in Fig. 4.6,

so the calibration for the carbon content will be easy. In Case III, the error is within ±25 MPa at its maximum and is acceptable for stress measurement.

When we use this method for stress measurement, the coefficients A and B have to be known in advance as accurate values. For the case of residual-stress measurement or applied-stress measurement of the structural members, the coefficients A and B can not be obtained from the measuring objects themselves. Therefore, the calibration methods of A and B should be the subject of further research.

REFERENCES FOR CHAPTER IV

[1] N. S. Akulov, Z. Physik, **69**, 822 (1931).

[2] R. Gans, Ann. Physik [5], **15**, 28 (1932).

[3] R. Becker and W. Döring, "Ferromagnetismus", Chap. 13 (1939) Springer, Berlin.

[4] T. Holstein and H. Primakoff, Phys. Rev., **59**, 388 (1941).

[5] H. Gengnagel and U. Hofmann, Phys. Stat. Sol., **29**, 91 (1968).

[6] E. Czerlinsky, Ann. Physik [5], **13**, 80 (1932).

[7] H. Polley, Ann. Physik [5], **36**, 625 (1939).

[8] R. Becker and W. Döring, "Ferromagnetismus", Chap. 11 (1939) Springer, Berlin.

[9] S. Chikazumi, "Physics of Ferromagnetism, vol. II", p. 266, (1984) Shokabo, Tokyo (in Japanese).

[10] S. Chikazumi, "Physics of Ferromagnetism, vol. II", p. 292, (1984) Shokabo, Tokyo (in Japanese).

[11] R. M. Bozorth, "Ferromagnetism", p. 820 (1951) D. van Nostrand, Princeton.

[12] E. W. Lee, Rep. Prog. Phys., **18**, 185 (1955).

[13] C. W. Chen, "Magnetism and Metallurgy of Soft Magnetic Materials", p. 109 (1986) Dover, Mineola, N.Y.

[14] W. J. Carr, Jr. and R. Somluchowski, Phys. Rev., **83**, 1236 (1951).

[15] J. Iwayanagi and S. Abuku, Proc. 11th Jpn. Cong. Test. Matr., 47 (1967).

[16] J. Iwayanagi and S. Abuku, Proc. 11th Jpn. Cong. Matr. Res., 116 (1968).

[17] J. Iwayanagi, Rep. Ship Res. Inst., **12**, 67 (1975) (in Japanese).

[18] Y. Tomono, Metal Phys., **3**, 171 (1957) (in Japanese).

CHAPTER V

BIAXIAL STRESS MEASUREMENT BY A MAGNETIC PROBE BASED ON THE LAW OF APPROACH TO SATURATION MAGNETIZATION

5.1 INTRODUCTION

In the previous chapter, effect of stress on the law of approach to saturation magnetization was examined, and the method for measuring stresses in steel bars was also proposed. The present chapter deals with the proposal of using the magnetic probe as a method applicable to steel plates based on the above mentioned law.

It is to be noted that up to the present magnetic method has not been demonstrated to measure the principal stresses in a biaxial state. Review of the work of Yoshinaga [1] and Langman [2] indicated independently that the method at a low field can measure the principal direction and the difference of principal stresses in a biaxial state, but not the principal stresses themselves. The method using Barkhausen noise has also the same performance as that at low field [3]. We have to employ the shear difference method, which is often used in photoelastic stress analysis, in order to obtain the principal stresses from the differences of those values. Unfortunately, the shear difference method is not practical nor applicable

to many cases because of the integration error and/or nonexistence of stress-free point near the measuring points.

On the other hand, the method at high field can measure directly the principal stresses based on the following equations: :

$$m_1 = A + B (\sigma_1 - 0.5 \sigma_2) \qquad (5.1a)$$

$$m_2 = A + B (\sigma_2 - 0.5 \sigma_1) \qquad (5.1b)$$

where σ_1, σ_2 are the principal stresses in a biaxial state, m_1 is the magnetic output in the direction of σ_1, m_2 in the direction of σ_2, and A and B are constants. These equations are derived by the fact that the volume magnetostriction is negligible compared with the linear magnetostriction in the region of $H < 80$ kA/m [4].

Iwayanagi [5] demonstrated that the stresses measured by a magnetic method in which eq. (5.1) was assumed corresponded with the stresses measured by X-ray diffraction method. However, there is yet no study which attend to measure the principal stresses of a biaxial state by using eq. (5.1).

This chapter proposes the apparatus for measuring stresses of steel plates based on the law of approach to saturation magnetization. By using the said apparatus both the uniaxial tensile stresses in a steel plate and the biaxial stresses in cruciform specimens were measured. The possibility of measuring the principal stresses is likewise discussed.

5.2 EXPERIMENTAL PROCEDURE

5.2.1 Apparatus

Figure 5.1 shows the magnetic probe used in this experiment. The probe has the same components as that shown in Chapter II, i.e., a probe yoke, three coils wound on the probe, and a Hall sensor attached on the specimen surface. Direct current passing through Bias coil produces biasing field in the specimen, and the biasing field strength H is measured by the Hall sensor. Alternative current produces alternative field, which is superimposed on the biasing field, and the alternative field strength h is also measured by the Hall sensor. The alternative flux ϕ induced in the specimen is measured from the voltage induced in the search coil. The search coil is wound only around the central piece of the probe yoke. The two outer yokes limit the flux flow of the central magnetic circuit. Only the flux whose direction is parallel to the measuring direction will be detected by using this "guard yoke system" [6-8]. The magnetic probe is refined to be able to produce high biasing field up to 80 kA/m and to achieve the smooth flow of flux.

Figure 5.2 shows a block diagram of the measuring apparatus. Direct current is supplied by a d.c. power supply, and alternative current is supplied by an a.c. power supply. A personal computer controls these power supplies to adjust the magnitude of the magnetizing currents. The voltage of direct current induced in the Hall sensor (denoted as V_H) is measured by a digital voltmeter and the value is sent to the computer. The voltage of alternative current induced in the Hall sensor

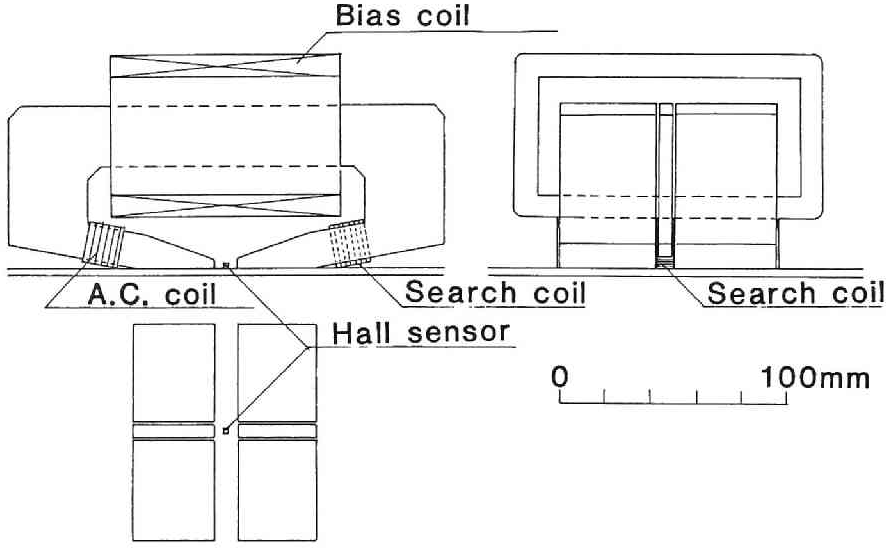

Fig. 5.1 Magnetic probe.

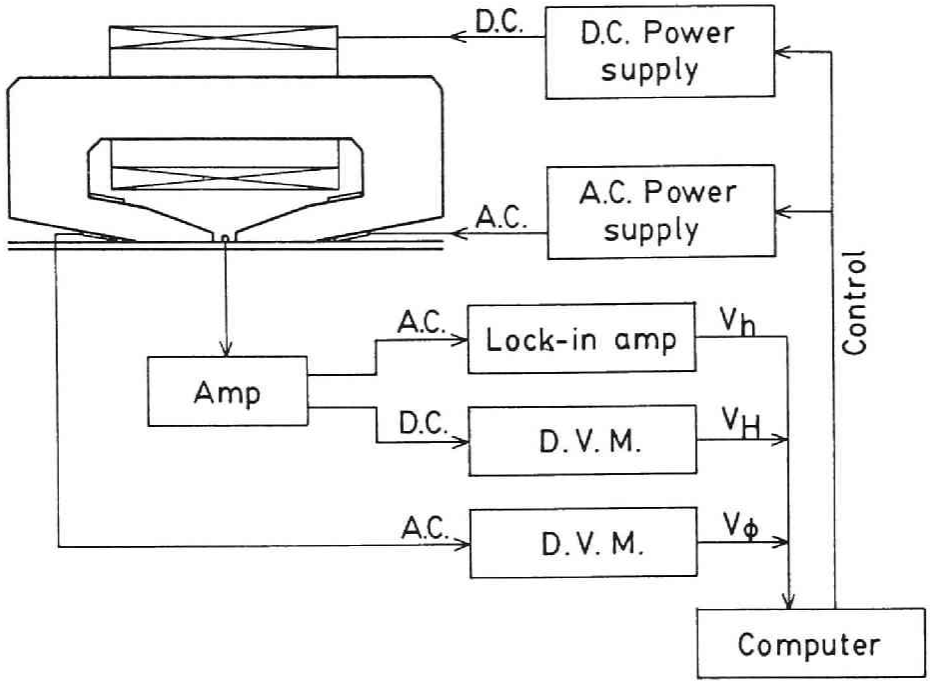

Fig. 5.2 Block diagram of the measuring setup.

(denoted as V_h) is measured by a lock-in amplifier and the value is also sent to the computer. These values of V_H and V_h, which are proportional to those of biasing field H and alternative field h, respectively, are fed back to adjust the magnitude of the magnetizing currents. The voltage of alternative current induced in the search coil (denoted as V_ϕ) is measured by a digital voltmeter and sent to the computer.

In this experiment, the values of V_ϕ/V_h were measured at biasing fields of H = 55.2, 58.6, 63.2, 69.5, 79.6 kA/m, which are arranged at the regular intervals in the dimension of $1/H^3$. The alternative magnetizing fields had a frequency of 1 kHz and the magnitude was adjusted to the value of 80 A/m (in r.m.s.).

5.2.2 Specimens and Loading Procedure

The specimen material used is a hot-rolled plate of low-carbon steel (JIS SS41). The specimen used for uniaxial tension test (Specimen 1) has a length of 600 mm, a width of 75 mm, and a thickness of 5.7 mm. Tensile stresses were applied below the elastic limit, and the measurement in the longitudinal direction (rolling direction) was performed at various stresses.

The specimens used for biaxial stress test, which have cruciform shape and a thickness of 3.2 mm, are shown in Fig. 5.3 (Specimens 2 and 3). The load in the horizontal direction and that in the vertical direction were applied independently to the cruciform specimens by using three hydraulic jacks. The applied loads were 12, 42, 72 kN for Specimen 2, and 20, 70,

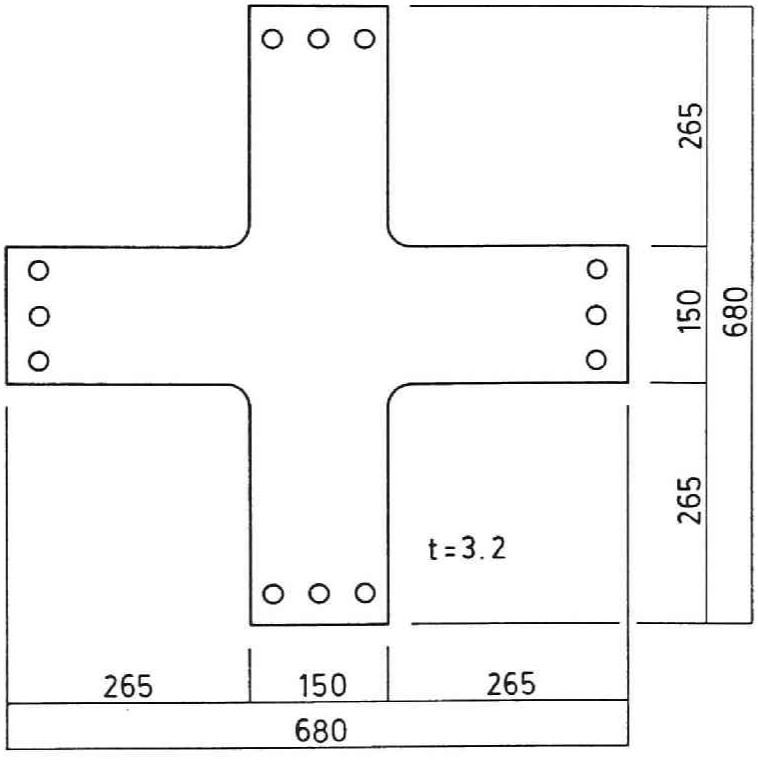

(a) Specimen 2

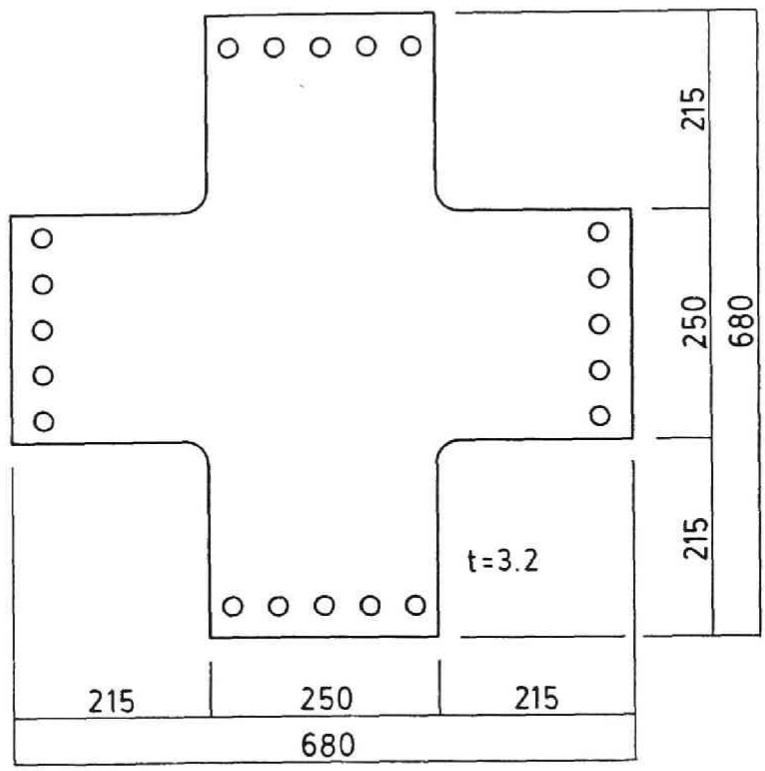

(b) Specimen 3

Fig. 5.3 Shape of the cruciform specimens for the biaxial stress test.

120 kN for Specimen 3. The applied stresses were measured by using strain gauges adhered on the back of the measured surface of the specimens. Measurement in the rolling direction (RD) and that in the perpendicular direction (TD) were carried out for each of the cruciform specimens.

5.3 EXPERIMENTAL RESULTS

5.3.1 Uniaxial Stress Test

Figure 5.4 shows the relationship between the value of V_ϕ/V_h and biasing field H in the dimension of $1/H^3$ for various applied stresses. It can be seen that V_ϕ/V_h varies linearly with $1/H^3$ and the slope of the curve in V_ϕ/V_h - $1/H^3$ relation (denoted as M) increases monotonously with an increase in applied stress.

Figure 5.5 shows a variation of square root of M with applied stresses. With an increase in stress, $\sqrt{M}$ increases linearly up to the maximum stress applied. Therefore, the relation can be expressed by a linear relation with respect to the applied stress σ as

$$\sqrt{M} = A + B\,\sigma \qquad (5.3)$$

where A and B are the constants, each of which is defined here as the initial value and the stress sensitivity, respectively. In this experiment, the coefficients were determined as $A = 0.948\times10^7\ (A/m)^{3/2}$ and $B = 2.40\times10^7\ (A/m)^{3/2}\ GPa^{-1}$. The relative stress sensitivity is thus determined as $B/A = 2.53\ GPa^{-1}$, which

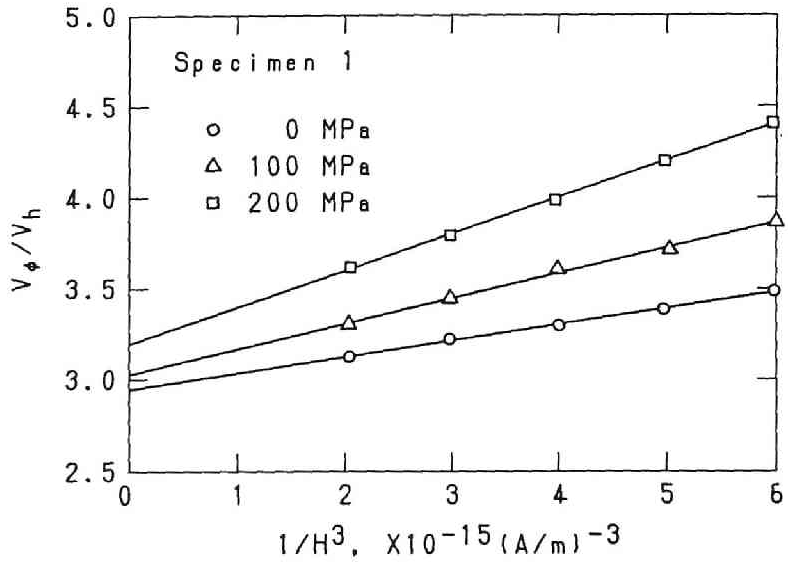

Fig. 5.4 Relationship between the value V_ϕ/V_h and biasing field H in the dimension of $1/H^3$ for uniaxial stress test (Specimen 1). The slope of the curve is represented by the symbol M.

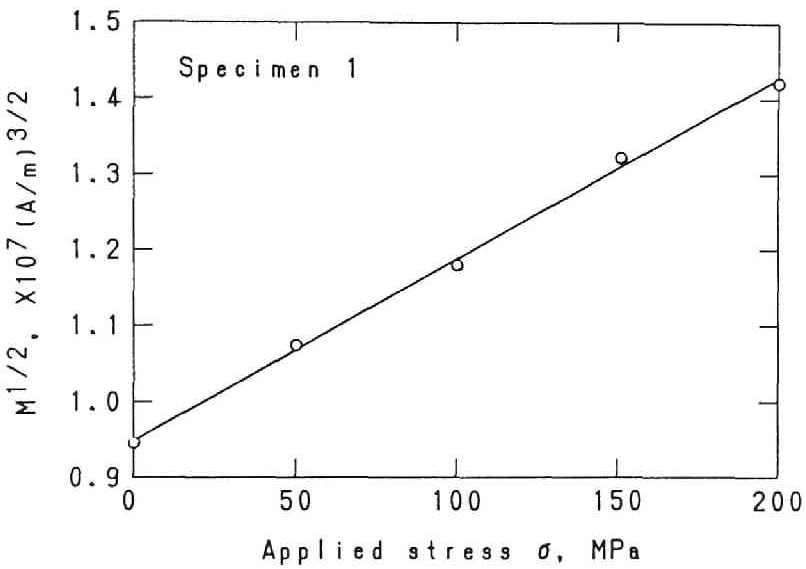

Fig. 5.5 Variation of $\sqrt{M}$ with applied stress σ for uniaxial stress test (Specimen 1).

is rather higher than the theoretical value of $B/A = 1.33\ GPa^{-1}$. The reason for the discrepancy is not clear. However it might be explained by the flux which fringes through the air.

Based on the results above, it is concluded that uniaxial stress in a steel plate can be determined by using the proposed method provided that coefficients A and B are known in advance.

5.3.2 Biaxial Stress Test

The relationship between the value of V_ϕ/V_h and $1/H^3$ is shown in Fig. 5.6. It can be seen in the same way as the uniaxial stress test that V_ϕ/V_h varies linearly with $1/H^3$. It can also be noted that the slope M increases monotonously with an increase in $\sigma_1 - 0.5\sigma_2$, where σ_1 and σ_2 indicate the principal stresses in the direction parallel and perpendicular to the measuring direction, respectively.

Figure 5.7 shows a variation of $\sqrt{M}$ with $\sigma_1 - 0.5\sigma_2$ of the applied stresses. It can be observed that $\sqrt{M}$ increases linearly with an increase in $\sigma_1 - 0.5\sigma_2$. This relation can be expressed as

$$\sqrt{M} = A + B\ (\ \sigma_1 - 0.5\ \sigma_2\ ) \qquad (5.3)$$

where A and B are constants. The theoretical formula of eq. (5.1) could thus be obtained in this experiment.

Table 5.1 illustrates the coefficients A and B for the biaxial test. The values of the relative sensitivity B/A are higher than the theoretical value of $B/A = 1.33\ GPa^{-1}$. The

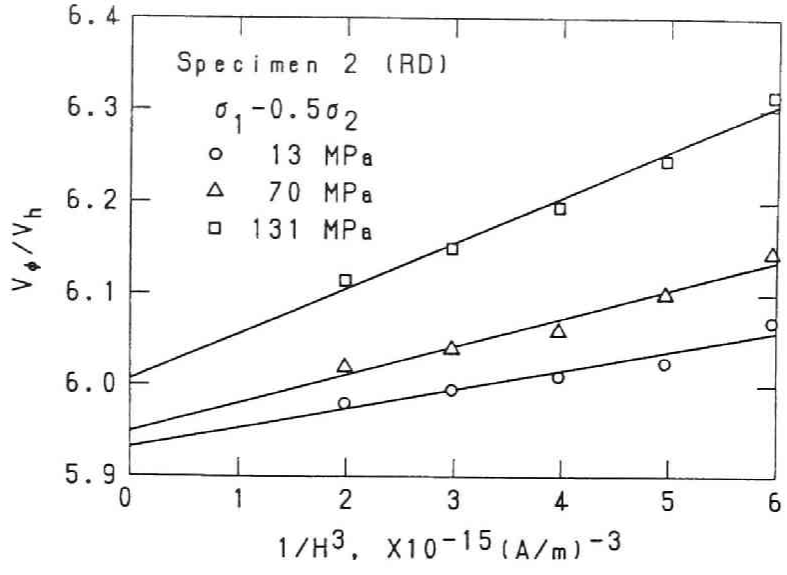

(a) Measured in the rolling direction of Specimen 2.

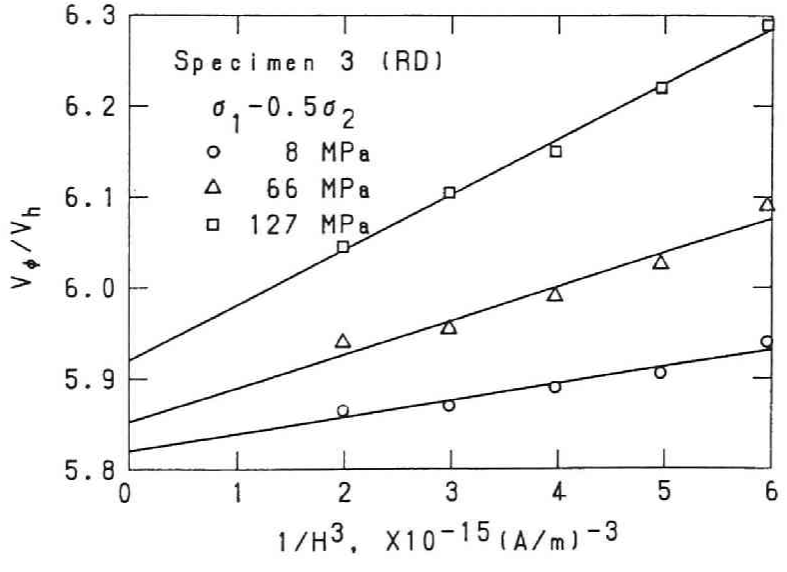

(b) Measured in the rolling direction of Specimen 3.

Fig. 5.6 Relationship between the magnetic output V_ϕ/V_h and $1/H^3$ for the biaxial stress test.

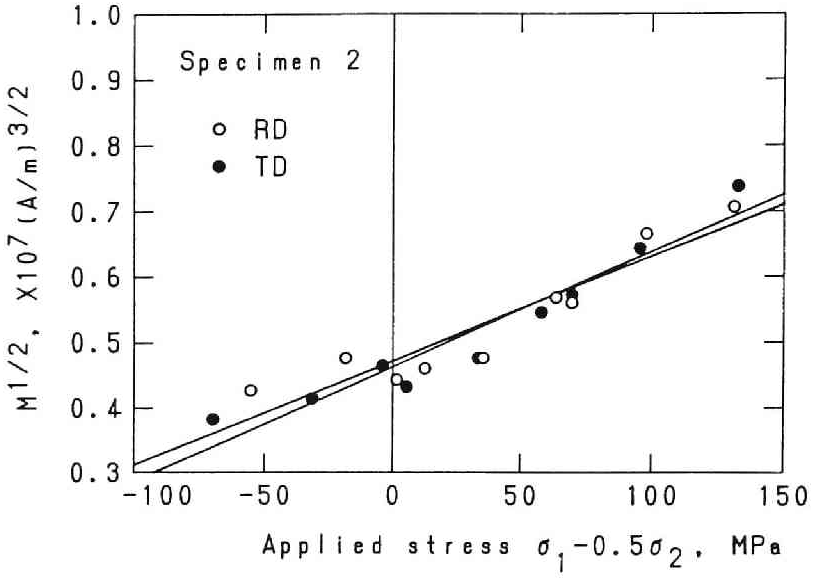

(a) Specimen 2.

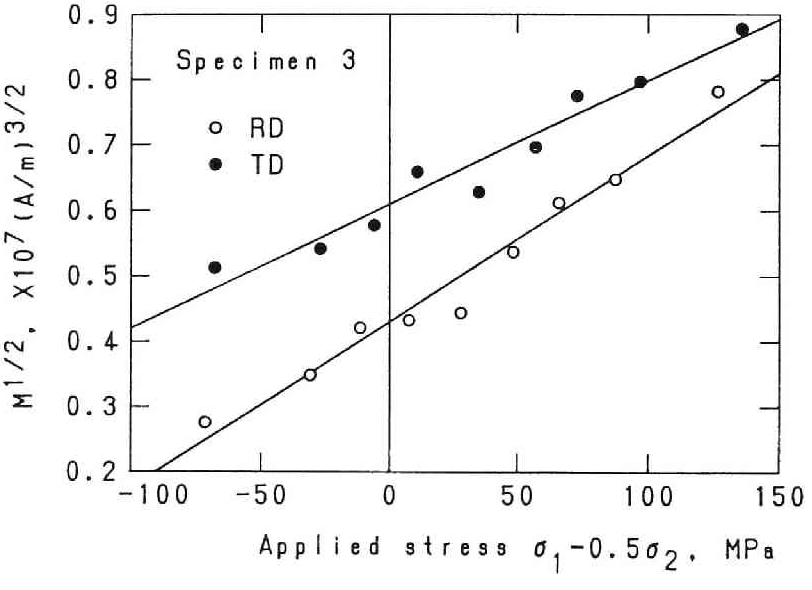

(b) Specimen 3.

Fig. 5.7 Variation of $\sqrt{M}$ with applied stresses $\sigma_1-0.5\sigma_2$, where σ_1 and σ_2 are the principal stresses of the measuring direction and the perpendicular direction, respectively.

values for Specimen 2 in the two directions (RD and TD) are almost the same for both the initial value A and the stress sensitivity B. However, the values for Specimen 3 are different for both A and B.

TABLE 5.1

COEFFICIENTS FOR THE BIAXIAL TEST

Specimen	A	B	B/A
	$(A/m)^{3/2}$	$(A/m)^{3/2}$ GPa^{-1}	GPa^{-1}
Specimen 2 (RD)	0.471×10^{7}	1.59×10^{7}	3.38
Specimen 2 (TD)	0.462	1.76	3.81
Specimen 3 (RD)	0.429	2.54	5.92
Specimen 3 (TD)	0.609	1.89	3.10

5.4 DISCUSSION

5.4.1 Influence of Rolling and Residual Stress

In this subsection, the nature of the difference of the coefficients A and B between RD and TD for Specimen 3 is discussed. As shown in Fig. 5.7 (a), the anisotropy caused by rolling cannot be seen for Specimen 2 because the $\sqrt{M}$ of the rolling direction (RD) and that of the perpendicular direction (TD) have the same values. Likewise, Specimen 3 which is made up of the same material as Specimen 2 cannot have the anisotropy caused by rolling. The resulting difference of $\sqrt{M}$ between RD and TD could be secondary to another factor which is further discussed below.

The probable nature of the anisotropy for Specimen 3 is residual stress. Now we assume that the difference of the

initial value A for Specimen 3 is caused only by the residual stresses. When the residual stresses are denoted as σ_{RD} for the rolling direction and σ_{TD} for the perpendicular direction, the initial values A_{RD} and A_{TD} including the effect of the residual stresses are expressed as

$$A_{RD} = A + B_{RD} (\sigma_{RD} - 0.5 \sigma_{TD}) \qquad (5.4a)$$

$$A_{TD} = A + B_{TD} (\sigma_{TD} - 0.5 \sigma_{RD}) \qquad (5.4b)$$

where the subscripts of RD and TD represent one in the rolling direction and in the perpendicular direction, respectively. The difference of those equations is derived as

$$A_{RD} - A_{TD} = (B_{RD}+0.5B_{TD}) \sigma_{RD} - (B_{TD}+0.5B_{RD}) \sigma_{TD} \qquad (5.5)$$

Substituting A_{RD}, A_{TD}, B_{RD} and B_{TD} for their experimental values given in Table 5.1, we obtain the value of the residual stress as

$$\sigma_{RD} - 0.91 \sigma_{TD} = -52 \text{ MPa} \qquad (5.6)$$

The value is acceptable for the residual stress produced in the specimen. The difference therefore of the initial value A in the measuring direction for Specimen 3 is most likewise due to residual stress.

The difference of the stress sensitivity B in the measuring direction may also be attributed to residual stress. However

this experiment was limited to clarifying its mechanism. More experimental observations are needed to elucidate this aspect.

5.4.2 Formula for Biaxial Stress State

The theoretical formula of eq. (5.1) was followed well for Specimen 2, but it was not followed for Specimen 3 because A and B had the different values between eqs. (5.1a) and (5.1b). However, we now assume that eq. (5.1) is generally followed and A and B are the constants determined for each material.

As shown in Fig. 5.8, the output m in the direction of θ from σ_1 will be given as

$$m = (m_1 + m_2)/2 + (m_1 - m_2)/2 \cos 2\theta \qquad (5.7)$$

where θ is the angle between the direction of σ_1 and the measuring direction. Substituting eq. (5.1) to eq. (5.7), we obtain

$$m = A + 0.25B(\sigma_1 + \sigma_2) + 0.75B(\sigma_1 - \sigma_2) \cos 2\theta \qquad (5.8)$$

Incidentally, the following equations are derived from the elastic theory [9]:

$$\sigma_p = (\sigma_1 + \sigma_2)/2 + (\sigma_1 - \sigma_2)/2 \cos 2\theta \qquad (5.9a)$$

$$\sigma_t = (\sigma_1 + \sigma_2)/2 - (\sigma_1 - \sigma_2)/2 \cos 2\theta \qquad (5.9b)$$

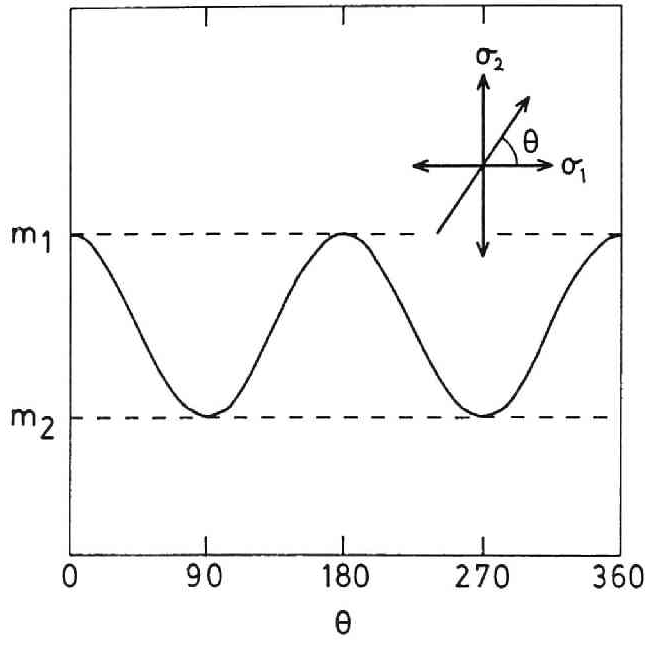

Fig. 5.8 Relationship between $\sqrt{M}$ and the measuring direction θ with respect to the direction of principal stresses. θ represents the angle between the measuring direction of the probe and the principal stress σ_1.

where σ_p and σ_t represent the normal stresses of which the direction are parallel and perpendicular to the measuring direction, respectively. Consequently, eq. (5.8) can be expressed as follows:

$$m = A + B (\sigma_p - 0.5 \sigma_t) \qquad (5.10)$$

This formula means that the magnetic output m depends on the normal stresses σ_p and σ_t and is independent of the shear stresses. Since it is derived from plausible assumptions, it is therefore necessary to carry out experiments in order to validate the formula.

5.5 CONCLUSIONS

The method using a magnetic probe based on the law of approach to saturation magnetization was proposed and the experiments using the magnetic probe and steel plates were carried out for uniaxial and biaxial stress state. The results obtained are summarized as follows:

(1) The value of V_ϕ/V_h varied linearly with $1/H^3$ and a square root of the slope $\sqrt{M}$ increased linearly with an increase in uniaxial applied stress. The relative stress sensitivity was 2.53 GPa^{-1}, which is rather higher than the theoretical value of 1.33 GPa^{-1}.

(2) The linear relation between V_ϕ/V_h and $1/H^3$ was also found for the biaxial test, and $\sqrt{M}$ increased linearly with an increase in σ_1-0.5σ_2, where σ_1 and σ_2 represent the principal

stresses in the direction parallel and perpendicular to the measuring direction, respectively. The initial value and the stress sensitivity were obtained for the rolling direction (RD) and the perpendicular direction (TD).

(3) The anisotropy which depended on the measuring direction was not observed for Specimen 2, so that the material anisotropy induced by rolling can be said to be small. The difference between the initial value of RD and that of TD which was observed for Specimen 3 was considered to be caused by residual stresses, and the value was estimated as $\sigma_{RD}-0.91\sigma_{TD} = -52$ MPa. The nature of the difference in the stress sensitivity was, however, not clarified.

(4) The formula, $m = A + B(\sigma_p-0.5\sigma_t)$, was deduced under some plausible assumptions, where m is the magnetic output in the arbitrary direction and σ_p and σ_t are the normal stresses in the direction parallel and perpendicular to the measuring direction, respectively.

In conclusion, uniaxial and biaxial stress in a steel plate can be measured by the method proposed in this chapter through the simple linear formula with respect to the stresses. The measurement of the principal stresses in a biaxial state can also be determined in principle.

REFERENCES FOR CHAPTER V

[1] A. Yoshinaga, Rep. Ship Res. Inst., **17**, 1 (1980) (in Japanese).

[2] R. Langman, NDT Int., **15**, 91 (1982).

[3] Y. Furuya, H. Shimada and Y. Ito, Hihakai Kensa, **36**, 530 (1987) (in Japanese).

[4] E. W. Lee, Rep. Prog. Phys., **18**, 185 (1955).

[5] J. Iwayanagi, Rep. Ship Res. Inst., **12**, 67 (1975) (in Japanese).

[6] F. J. Wilkins and A. E. Drake, Proc. Inst. Electr. Eng., **112**, 786 (1965).

[7] F. J. Wilkins and A. E. Drake, Proc. Inst. Electr. Eng., **117**, 1048 (1970).

[8] R. Langman, NDT Int., **14**, 255 (1981).

[9] S. P. Timoshenko and D. H. Young, "Elements of Strength of Materials", 5th ed., p. 59 (1968) Maruzen, Tokyo (Reprint of D. van Nostrand).

CHAPTER VI

SUMMARY AND CONCLUSIONS

This paper investigated the nondestructive stress measurement method utilizing magnetostriction for the application to steel structural members. This final chapter summarizes the results obtained through experiment and recommends further researches in the application of the method.

In Chapter II, a new kind of magnetic probe was developed for measuring the stresses of steel plates based on the variation of the reversible permeability in high magnetic fields. It was indicated that the stress of the specimen whose width is the same as that of the probe can be measured by the method described. However, when the width of the specimen is wider than that of the probe, stress can not be determined by this method because of the hysteresis phenomenon, and therefore, this phenomenon must first be solved prior to the application of the method to steel structural members.

In Chapter III, the hysteresis phenomenon of magnetization due to stress was investigated by employing a solenoid coil and a rod specimen in order to clarify the nature of the phenomenon. The experimental results showed that the reversible permeability was determined as a unique value when the biasing

field was higher than the critical value. Theoretical discussions were also performed on the basis of the stability of magnetization vectors determined by the equilibrium of the free energies. The theory predicted that the critical field H_{crit} as $H_{crit} = (2K + 3\lambda_{100}\sigma)/I_s$, where K is the cubic anisotropy constant, λ_{100} the magnetostriction constant, σ the stress, and I_s the spontaneous magnetization. It agreed well with the experimental results, wherein it was concluded that the biasing field should be above the critical field.

In Chapter IV, the effect of stress on magnetization in high fields was examined on the basis of the law of approach to saturation magnetization. Theoretical formulas of the reversible permeability μ_{rev} under the biasing field H were deduced as

$$\mu_{rev} = 1 + M/H^3,$$

$$\sqrt{M} = A + B\,\sigma,$$

$$A = 348\ K / \sqrt{I_s},$$
$$B = 522\ (\lambda_{100} - \lambda_{111}) / \sqrt{I_s},$$

where λ_{111} is the magnetostriction constant. In order to verify the formulas, specimens which were different in chemical composition and heat treatment were examined. The experimental values of I_s, K, and $(\lambda_{100}-\lambda_{111})$ obtained by using the formulas agreed fairly well with the standard values. The formulas

therefore were verified by this experiment. The measurement error of stress by the method based on the formulas was examined and it was concluded that the coefficients A and B should be predicted accurately. It follows therefore that the factors affecting A and B should be studied in further researches and a calibration method be developed for this purpose.

In Chapter V, the probe method for measuring stresses of steel plates were proposed on the basis of the formulas described in Chapter IV. The biaxial stresses were also measured by the magnetic probe in the directions of the principal stresses. The results showed that the magnetic output m varied linearly with the applied stresses and could be expressed as

$$m_1 = A + B (\sigma_1 - 0.5 \sigma_2),$$

where m_1 is the magnetic output in the direction of σ_1, and σ_1 and σ_2 are the principal stresses. Therefore, the principal stresses can be determined directly from the measured values in the direction of σ_1 and σ_2. Moreover, the following relation for a biaxial stress state was deduced under some plausible assumptions as

$$m = A + B (\sigma_p - 0.5 \sigma_t),$$

where m is the magnetic output in the arbitrary direction, and σ_p and σ_t are the normal stresses parallel and perpendicular to the measuring direction, respectively. This indicates that

the magnetic output is independent of the shear stresses.

Through this study, a new kind of stress measurement method was obtained based on the law of approach to saturation magnetization. The method proposed here has several advantages because it is based on the domain theory; the fundamental formula is a linear relation of stress; the reproducibility of the measured value is good; and the influence of material nature is small.

The use of this method to nondestructive stress measurement of steel structural members can be further explored through future researches such as the following:

(1) The application of the method to various materials and how influence material nature such as chemical composition, plastic deformation, heat treatment, texture anisotropy by rolling on the coefficients A and B.

(2) The development of a measuring apparatus processing high precision and stability (reproducibility) characteristics.

(3) The application of the method for estimating the measurement error thorough an experiment using a structural member such as rolled H-beam.

(4) Field application as a practical approach to estimate the suitability of this method.